

### Online supplemental material

Figure S1 shows renal cysts in kidney sections from adult and embryonic *MALS-3<sup>9/9</sup>* mice as well as urine concentrating ability in mutant mice. Figure S2 shows the colocalization of MALS and DLG with the tight junction. Figure S3 shows partial disruption of polarity complexes in collecting ducts of *MALS-3<sup>9/9</sup>*. Figure S4 shows that localization of PAR-3, aPKC, and SCRIB does not require MALS-3. Figure S5 depicts the generation and characterization of the *MALS-3* floxed allele. Online supplemental material is available at <http://www.jcb.org/cgi/content/full/jcb.200702054/DC1>.

The authors wish to thank Uta Grieshammer for assisting with study of embryonic mice and Zoltan Laskiz and Stephen Gluck for assisting with the renal pathology as well as Keith Mostov, Louis Reichardt, Michael Caplan, David Pearce, and Vivek Bhalla for their critical reading of the manuscript. The authors declare there is no financial conflict of interest related to this work.

This work was supported by grants from the National Institutes of Health (to D.S. Bredt and O. Olsen) and the Research Grant Council of Hong Kong (to M. Zhang).

Submitted: 8 February 2007

Accepted: 11 September 2007

## REFERENCES

- Bachmann, A., M. Schneider, E. Theilenberg, F. Grawe, and E. Knust. 2001. *Drosophila* Stardust is a partner of Crumbs in the control of epithelial cell polarity. *Nature*. 414:638–643.
- Bachmann, A., M. Timmer, J. Sierralta, G. Pietrini, E.D. Gundelanger, E. Knust, and U. Thomas. 2004. Cell type-specific recruitment of *Drosophila* Lin-7 to distinct MAGUK-based protein complexes defines novel roles for Sdt and Dlg-S97. *J. Cell Sci.* 117:1899–1909.
- Betschinger, J., K. Mechler, and J.A. Knoblich. 2003. The Par complex directs asymmetric cell division by phosphorylating the cytoskeletal protein Lgl. *Nature*. 422:326–330.
- Bhat, M.A., S. Izaddoost, Y. Lu, K.O. Cho, K.W. Choi, and H.J. Bellen. 1999. Discs Lost, a novel multi-PDZ domain protein, establishes and maintains epithelial polarity. *Cell*. 96:833–845.
- Bilder, D., and N. Perrimon. 2000. Localization of apical epithelial determinants by the basolateral PDZ protein Scribble. *Nature*. 403:676–680.
- Bilder, D., M. Li, and N. Perrimon. 2000. Cooperative regulation of cell polarity and growth by *Drosophila* tumor suppressors. *Science*. 289:113–116.
- Borg, J.-P., M.O. López-Figueroa, M. de Taddèo-Borg, D.E. Kroon, R.S. Turner, S.J. Watson, and B. Ben Margolis. 1999. Molecular analysis of the X11-mLin-2/CASK complex in brain. *J. Neurosci.* 19:1307–1316.
- Bouby, N., S. Bachmann, D. Bichet, and L. Bankir. 1990. Effect of water intake on the progression of chronic renal failure in the 5/6 nephrectomized rat. *Am. J. Physiol.* 258:F973–F979.
- Bouby, N., M. Ahloulay, E. Nsegbe, M. Déchaux, F. Schmitt, and L. Bankir. 1996. Vasopressin increases glomerular filtration rate in conscious rats through its antidiuretic action. *J. Am. Soc. Nephrol.* 7:842–851.
- Butz, S., M. Okamoto, and T.C. Sudhof. 1998. A tripartite protein complex with the potential to couple synaptic vesicle exocytosis to cell adhesion in brain. *Cell*. 94:773–782.
- Campo, C., A. Mason, D. Maouyo, O. Olsen, D. Yoo, and P.A. Welling. 2005. Molecular mechanisms of membrane polarity in renal epithelial cells. *Rev. Physiol. Biochem. Pharmacol.* 153:47–99.
- Chang, C.P., B.W. McDill, J.R. Neilson, H.E. Joist, J.A. Epstein, G.R. Crabtree, and F. Chen. 2004. Calcineurin is required in urinary tract mesenchyme for the development of the pyeloureteral peristaltic machinery. *J. Clin. Invest.* 113:1051–1058.
- Djiane, A., S. Yogev, and M. Mlodzik. 2005. The apical determinants aPKC and Patj regulate Frizzled-dependent planar cell polarity in the *Drosophila* eye. *Cell*. 121:621–631.
- Dressler, G.R. 2006. The cellular basis of kidney development. *Annu. Rev. Cell Dev. Biol.* 22:509–529.
- Etemad-Moghadam, B., S. Guo, and K.J. Kemphues. 1995. Asymmetrically distributed PAR-3 protein contributes to cell polarity and spindle alignment in early *C. elegans* embryos. *Cell*. 83:743–752.
- Fan, S., T.W. Hurd, C.J. Liu, S.W. Straight, T. Weimbs, E.A. Hurd, S.E. Domino, and B. Margolis. 2004. Polarity proteins control ciliogenesis via kinesin motor interactions. *Curr. Biol.* 14:1451–1461.
- Feng, W., J.F. Long, J.S. Fan, T. Suetake, and M. Zhang. 2004. The tetrameric L27 domain complex as an organization platform for supramolecular assemblies. *Nat. Struct. Mol. Biol.* 11:475–480.
- Feng, W., J.F. Long, and M. Zhang. 2005. A uniAed assembly mode revealed by the structures of tetrameric L27 domain complexes formed by mLin-2/mLin-7 and Patj/Pals1 scaffold proteins. *Proc. Natl. Acad. Sci. USA*. 102:6861–6866.
- Gateff, E., and H.A. Schneiderman. 1969. Neoplasms in mutant and cultured wild-type tissues of *Drosophila*. *Natl. Cancer Inst. Monogr.* 31:365–397.
- Grieshammer, U., C. Cebrian, R. Ilagan, E. Meyers, D. Herzlinger, and G.R. Martin. 2005. FGF8 is required for cell survival at distinct stages of nephrogenesis and for regulation of gene expression in nascent nephrons. *Development*. 132:3847–3857.
- Hildebrandt, F., and W. Zhou. 2007. Nephronophthisis-associated ciliopathies. *J. Am. Soc. Nephrol.* 18:1855–1871.
- Hong, Y., B. Stronach, N. Perrimon, L.Y. Jan, and Y.N. Jan. 2001. *Drosophila* Stardust interacts with Crumbs to control polarity of epithelia but not neuroblasts. *Nature*. 414:634–638.
- Hurd, T.W., L. Gao, M.H. Roh, L.G. Macara, and B. Margolis. 2003. Direct interaction of two polarity complexes implicated in epithelial tight junction assembly. *Nat. Cell Biol.* 5:137–142.
- Izumi, Y., T. Hirose, Y. Tamai, S. Hirai, Y. Nagashima, T. Fujimoto, Y. Tabuse, K.J. Kemphues, and S. Ohno. 1998. An atypical PKC directly associates and colocalizes at the epithelial tight junction with ASIP, a mammalian homologue of *Caenorhabditis elegans* polarity protein PAR-3. *J. Cell Biol.* 143:95–106.
- Jo, K., R. Derin, M. Li, and D.S. Bredt. 1999. Characterization of MALS/Vel1-1, -2, and -3: a family of mammalian LIN-7 homologs enriched at brain synapses in association with the postsynaptic density-95/NMDA receptor postsynaptic complex. *J. Neurosci.* 19:4189–4199.
- Joberty, G., C. Petersen, L. Gao, and I.G. Macara. 2000. The cell-polarity protein Par6 links Par3 and atypical protein kinase C to Cdc42. *Nat. Cell Biol.* 2:531–539.
- Kaech, S.M., C.W. Whitfield, and S.K. Kim. 1998. The LIN-2/LIN-7/LIN-10 complex mediates basolateral membrane localization of the *C. elegans* EGF receptor LET-23 in vulval epithelial cells. *Cell*. 94:761–771.
- Kalluri, R., and E.G. Neilson. 2003. Epithelial-mesenchymal transition and its implications for Abrosis. *J. Clin. Invest.* 112:1776–1784.
- Kamberov, E., O. Makarova, M. Roh, A. Liu, D. Karnak, S. Straight, and B. Margolis. 2000. Molecular cloning and characterization of Pals, proteins associated with mLin-7. *J. Biol. Chem.* 275:11425–11431.
- Koseki, C., D. Herzlinger, and Q. al-Awqati. 1992. Apoptosis in metanephric development. *J. Cell Biol.* 119:1327–1333.
- Lee, D.B., E. Huang, and H.J. Ward. 2006. Tight junction biology and kidney dysfunction. *Am. J. Physiol. Renal Physiol.* 290:F20–F34.
- Lee, J.M., S. Dedhar, R. Kalluri, and E.W. Thompson. 2006. The epithelial-mesenchymal transition: new insights in signaling, development, and disease. *J. Cell Biol.* 172:973–981.
- Lee, S., S. Fan, O. Makarova, S. Straight, and B. Margolis. 2002. A novel and conserved protein-protein interaction domain of mammalian Lin-2/CASK binds and recruits SAP97 to the lateral surface of epithelia. *Mol. Cell Biol.* 22:1778–1791.
- Leonoudakis, D., L.R. Conti, C.M. Radeke, L.M. McGuire, and C.A. Vandenberg. 2004. A multiprotein trafficking complex composed of SAP97, CASK, Veli, and Mint1 is associated with inward rectifier Kir2 potassium channels. *J. Biol. Chem.* 279:19051–19063.
- Li, J., F. Chen, and J.A. Epstein. 2000. Neural crest expression of Cre recombinase directed by the proximal Pax3 promoter in transgenic mice. *Genesis*. 26:162–164.
- Li, Y., D. Karnak, B. Demeler, B. Margolis, and A. Lavie. 2004. Structural basis for L27 domain-mediated assembly of signaling and cell polarity complexes. *EMBO J.* 23:2723–2733.
- Lin, D., A.S. Edwards, J.P. Fawcett, G. Mbamalu, J.D. Scott, and T. Pawson. 2000. A mammalian PAR-3-PAR-6 complex implicated in Cdc42/Rac1 and aPKC signalling and cell polarity. *Nat. Cell Biol.* 2:540–547.
- Medina, E., J. Williams, E. Klipfell, D. Zarnescu, G. Thomas, and A. Le Bivic. 2002. Crumbs interacts with moesin and beta(Heavy)-spectrin in the apical membrane skeleton of *Drosophila*. *J. Cell Biol.* 158:941–951.
- Misawa, H., Y. Kawasaki, J. Mellor, N. Sweeney, K. Jo, R.A. Nicoll, and D.S. Bredt. 2001. Contrasting localizations of MALS/LIN-7 PDZ proteins in brain and molecular compensation in knockout mice. *J. Biol. Chem.* 276:9264–9272.
- Okamoto, M., and T.C. Sudhof. 1997. Mints, Munc18-interacting proteins in synaptic vesicle exocytosis. *J. Biol. Chem.* 272:31459–31464.
- Olsen, O., H. Liu, J.B. Wade, J. Merot, and P.A. Welling. 2002. Basolateral membrane expression of the Kir 2.3 channel is coordinated by PDZ interaction with Lin-7/CASK complex. *Am. J. Physiol. Cell Physiol.* 282:C183–C195.
- Olsen, O., K.A. Moore, M. Fukata, T. Kazuta, J.C. Trinidad, F.W. Kauer, M. Streuli, H. Misawa, A.L. Burlingame, R.A. Nicoll, and D.S. Bredt. 2005a.

- Neurotransmitter release regulated by a MALS-liprin-alpha presynaptic complex. *J. Cell Biol.* 170:1127–1134.
- Olsen, O., J.B. Wade, N. Morin, D.S. Bredt, and P.A. Welling. 2005b. Differential localization of mammalian Lin-7 (MALS/Veli) PDZ proteins in the kidney. *Am. J. Physiol. Renal Physiol.* 288:F345–F352.
- Omori, Y., and J. Malicki. 2006. *oko meduzy* and related crumbs genes are determinants of apical cell features in the vertebrate embryo. *Curr. Biol.* 16:945–957.
- Perego, C., C. Vanoni, A. Villa, R. Longhi, S.M. Kaech, E. Frohli, A. Hajnal, S.K. Kim, and G. Pietrini. 1999. PDZ-mediated interactions retain the epithelial GABA transporter on the basolateral surface of polarized epithelial cells. *EMBO J.* 18:2384–2393.
- Perego, C., C. Vanoni, S. Massari, R. Longhi, and G. Pietrini. 2000. Mammalian LIN-7 PDZ proteins associate with beta-catenin at the cell-cell junctions of epithelia and neurons. *EMBO J.* 19:3978–3989.
- Plant, P.J., J.P. Fawcett, D.C. Lin, A.D. Holdorf, K. Binns, S. Kulkarni, and T. Pawson. 2003. A polarity complex of mPar-6 and atypical PKC binds, phosphorylates and regulates mammalian Lgl. *Nat. Cell Biol.* 5:301–308.
- Roh, M.H., O. Makarova, C.J. Liu, K. Shin, S. Lee, S. Laurinec, M. Goyal, R. Wiggins, and B. Margolis. 2002. The Maguk protein, Pals1, functions as an adapter, linking mammalian homologues of Crumbs and Discs Lost. *J. Cell Biol.* 157:161–172.
- Schneeberger, E.E., and R.D. Lynch. 1992. Structure, function, and regulation of cellular tight junctions. *Am. J. Physiol.* 262:L647–L661.
- Segbert, C., K. Johnson, C. Theres, D. van Furden, and O. Bossinger. 2004. Molecular and functional analysis of apical junction formation in the gut epithelium of *Caenorhabditis elegans*. *Dev. Biol.* 266:17–26.
- Shelly, M., Y. Mosesson, A. Citri, S. Lavi, Y. Zwang, N. Melamed-Book, B. Aroeti, and Y. Yarden. 2003. Polar expression of ErbB-2/HER2 in epithelia. Bimodal regulation by Lin-7. *Dev. Cell.* 5:475–486.
- Shin, K., V.C. Fogg, and B. Margolis. 2006. Tight junctions and cell polarity. *Annu. Rev. Cell Dev. Biol.* 22:207–235.
- Simons, M., and G. Walz. 2006. Polycystic kidney disease: cell division without a clue? *Kidney Int.* 70:854–864.
- Simske, J.S., S.M. Kaech, S.A. Harp, and S.K. Kim. 1996. LET-23 receptor localization by the cell junction protein LIN-7 during *C. elegans* vulval induction. *Cell.* 85:195–204.
- Straight, S.W., D. Karnak, J.P. Borg, E. Kamberov, H. Dare, B. Margolis, and J.B. Wade. 2000. mLin-7 is localized to the basolateral surface of renal epithelia via its NH(2) terminus. *Am. J. Physiol. Renal Physiol.* 278:F464–F475.
- Straight, S.W., L. Chen, D. Karnak, and B. Margolis. 2001. Interaction with mLin-7 alters the targeting of endocytosed transmembrane proteins in mammalian epithelial cells. *Mol. Biol. Cell.* 12:1329–1340.
- Straight, S.W., J.N. Pieczynski, E.L. Whiteman, C.J. Liu, and B. Margolis. 2006. Mammalian lin-7 stabilizes polarity protein complexes. *J. Biol. Chem.* 281:37738–37747.
- Tabuse, Y., Y. Izumi, F. Piano, K.J. Kemphues, J. Miwa, and S. Ohno. 1998. Atypical protein kinase C cooperates with PAR-3 to establish embryonic polarity in *Caenorhabditis elegans*. *Development.* 125:3607–3614.
- Tepass, U., C. Theres, and E. Knust. 1990. crumbs encodes an EGF-like protein expressed on apical membranes of *Drosophila* epithelial cells and required for organization of epithelia. *Cell.* 61:787–799.
- Tepass, U., G. Tanentzapf, R. Ward, and R. Fehon. 2001. Epithelial cell polarity and cell junctions in *Drosophila*. *Annu. Rev. Genet.* 35:747–784.
- Topinka, J.R., and D.S. Bredt. 1998. N-terminal palmitoylation of PSD-95 regulates association with cell membranes and interaction with K<sup>+</sup> channel Kv1.4. *Neuron.* 20:125–134.
- Torres, V.E., P.C. Harris, and Y. Pirson. 2007. Autosomal dominant polycystic kidney disease. *Lancet.* 369:1287–1301.
- Van Itallie, C.M., and J.M. Anderson. 2004. The molecular physiology of tight junction pores. *Physiology (Bethesda).* 19:331–338.
- Watts, J.L., B. Etemad-Moghadam, S. Guo, L. Boyd, B.W. Draper, C.C. Mello, J.R. Priess, and K.J. Kemphues. 1996. par-6, a gene involved in the establishment of asymmetry in early *C. elegans* embryos, mediates the asymmetric localization of PAR-3. *Development.* 122:3133–3140.
- Woods, D.F., and P.J. Bryant. 1991. The discs-large tumor suppressor gene of *Drosophila* encodes a guanylate kinase homolog localized at septate junctions. *Cell.* 66:451–464.
- Yu, J., T.J. Carroll, and A.P. McMahon. 2002. Sonic hedgehog regulates proliferation and differentiation of mesenchymal cells in the mouse metanephric kidney. *Development.* 129:5301–5312.

## Astrocytes as determinants of disease progression in inherited amyotrophic lateral sclerosis

Koji Yamanaka<sup>1,2</sup>, Seung Joo Chun<sup>1</sup>, Severine Boillee<sup>1</sup>, Noriko Fujimori-Tonou<sup>2</sup>, Hirofumi Yamashita<sup>2</sup>, David H Gutmann<sup>3</sup>, Ryosuke Takahashi<sup>4</sup>, Hidemi Misawa<sup>5</sup> & Don W Cleveland<sup>1</sup>

**Dominant mutations in superoxide dismutase cause amyotrophic lateral sclerosis (ALS), an adult-onset neurodegenerative disease that is characterized by the loss of motor neurons. Using mice carrying a deletable mutant gene, diminished mutant expression in astrocytes did not affect onset, but delayed microglial activation and sharply slowed later disease progression. These findings demonstrate that mutant astrocytes are viable targets for therapies for slowing the progression of non-cell autonomous killing of motor neurons in ALS.**

ALS is an adult-onset neurodegenerative disease, characterized by a progressive and fatal loss of motor neurons. Dominant mutations in the gene for superoxide dismutase (*SOD1*) are the most frequent cause of inherited ALS. Ubiquitous expression of mutant *SOD1* in rodents leads to progressive, selective motor neuron degeneration as a result of acquired toxic properties. The exact mechanism responsible for motor neuron degeneration in ALS, however, is not known<sup>1,2</sup>. Mutant damage in the vulnerable motor neurons is a key determinant of disease onset<sup>3</sup>, whereas accumulating evidence supports an active role of non-neuronal cells in motor neuron degeneration<sup>3-7</sup>. Evidence with selective gene excision<sup>3</sup> or bone-marrow grafting<sup>5</sup> has demonstrated that mutant *SOD1*-derived damage in microglia accelerates later disease progression. Despite the importance of astrocyte function, the role of mutant action in astrocytes in disease has not been tested *in vivo*.

To examine whether mutant *SOD1* damage in astrocytes contributes to disease, *loxSOD1*<sup>G37R</sup> mice<sup>3</sup>, carrying a mutant *SOD1* gene that can be deleted by the action of the Cre recombinase, were mated with *GFAP-Cre* mice (Fig. 1 and Supplementary Fig. 1 online), which express both Cre recombinase and  $\beta$ -galactosidase (*LacZ*) under the control of the human *GFAP* promoter<sup>8</sup>. Mice from these matings that carry the *GFAP-Cre* transgene are denoted as Cre<sup>+</sup>, whereas mice without it are referred to as Cre<sup>-</sup>. To determine the cell-type specificity of Cre expression in the spinal cord, *GFAP-Cre* mice were mated to Rosa26 mice, which ubiquitously express a *LacZ* gene that encodes

functional  $\beta$ -galactosidase only after Cre-mediated recombination. Although this *GFAP-Cre* transgene is expressed in a subset of neurons in the cerebellum and hippocampus during embryogenesis<sup>9</sup>, measurement of  $\beta$ -galactosidase activity (by deposition of a blue reaction product after addition of the X-gal substrate) demonstrated that Cre expression and Cre-mediated recombination was restricted in the spinal cord to *GFAP*-reactive astrocytes (Fig. 1a,b). The efficiency of mutant gene excision in cultured astrocytes from newborn *loxSOD1*<sup>G37R</sup>/*GFAP-Cre*<sup>+</sup> mice was ~76% (Fig. 1d,e), determined by quantitative PCR for human *SOD1* transgene number (Fig. 1d) and immunoblotting for mutant *SOD1* levels (Fig. 1e). We observed neither detectable Cre activity nor mutant gene excision in microglia (Fig. 1c and Supplementary Fig. 2 online).

A simple, objective measure of disease onset and early disease was applied by initiation of weight loss, itself reflecting denervation-induced muscle atrophy. Reduction of *SOD1*<sup>G37R</sup> in astrocytes did not slow disease onset nor early disease (*GFAP-Cre*<sup>+</sup>, 341.6  $\pm$  48.9 d; *GFAP-Cre*<sup>-</sup>, 337.0  $\pm$  35.8 d; Fig. 1f,h). However, late disease progression (from early disease to end stage) was sharply delayed, providing a mean extension of survival by 48 d (Cre<sup>+</sup>, 87.4 d; Cre<sup>-</sup>, 39.5 d; Fig. 1j). Progression from onset to early disease was more modestly slowed by 14 d (Cre<sup>+</sup>, 99.3 d; Cre<sup>-</sup>, 85.2 d; Fig. 1i). Overall survival was extended by 60 d (Cre<sup>+</sup>, 436.5  $\pm$  38.8 d; Cre<sup>-</sup>, 376.5  $\pm$  26.9 d; Fig. 1g). This contrasts with delayed disease onset from diminished mutant synthesis solely within motor neurons (with a *VAcHT-Cre* transgene carrying the motor neuron-specific vesicular acetylcholine transporter promoter) without affecting disease progression (Supplementary Results, Supplementary Methods and Supplementary Fig. 3 online), just as reported previously with an *Isl1* (*Islet1*)-*Cre* transgene that is expressed in motor neurons and some peripheral tissues<sup>3</sup>.

Astrocytic and microglial cell activation is a well-accepted feature of *SOD1* mutant-mediated ALS<sup>1,2</sup>. An elevated proportion of *GFAP*-positive astrocytes appeared before disease onset (Fig. 2a) in *loxSOD1*<sup>G37R</sup> mice. This astrogliosis was progressive, readily apparent by onset (Fig. 2b) and more prominent during disease progression (Fig. 2c). Despite substantial mutant reduction, astrogliosis was not, however, different in comparing disease-matched *loxSOD1*<sup>G37R</sup>/*GFAP-Cre*<sup>+</sup> mice (Fig. 2d,e) and *loxSOD1*<sup>G37R</sup>/*GFAP-Cre*<sup>-</sup> mice (Fig. 2b,c).

Microglial activation occurred at earliest disease onset in Cre<sup>-</sup> mice (Fig. 2g) and was progressively more prominent during disease progression (Fig. 2h). Microglial activation was, however, substantially delayed from onset through early disease in the *GFAP-Cre*<sup>+</sup> mice when mutant *SOD1* levels were reduced only in astrocytes (Fig. 2i,j). By exploiting the presence of  $\beta$ -galactosidase to mark astrocytes with diminished *SOD1* mutant synthesis, examination of sections through-out lumbar spinal cords of symptomatic *loxSOD1*<sup>G37R</sup>/*GFAP-Cre*<sup>+</sup> mice

<sup>1</sup>Ludwig Institute for Cancer Research and Department of Medicine and Neuroscience, University of California at San Diego, 9500 Gilman Drive, La Jolla, California 92093-0670, USA. <sup>2</sup>Yamanaka Research Unit, RIKEN Brain Science Institute, 2-1 Hirosawa, Wako, Saitama 351-0198, Japan. <sup>3</sup>Department of Neurology, Washington University School of Medicine, 660 South Euclid Avenue, St. Louis, Missouri 63110, USA. <sup>4</sup>Department of Neurology, Graduate School of Medicine, Kyoto University, 54 Shogoin Kawahara-cho, Sakyo-ku, Kyoto 606-8507, Japan. <sup>5</sup>Department of Pharmacology, Kyoritsu University of Pharmacy, 1-5-30 Shibakoen, Minato-ku, Tokyo 105-8512, Japan. Correspondence should be addressed to D.W.C. (dcleveland@ucsd.edu) or K.Y. (kyamanaka@brain.riken.jp).

Received 26 November 2007; accepted 7 January 2008; published online 3 February 2008; doi:10.1038/nn2047



BRIEF COMMUNICATIONS

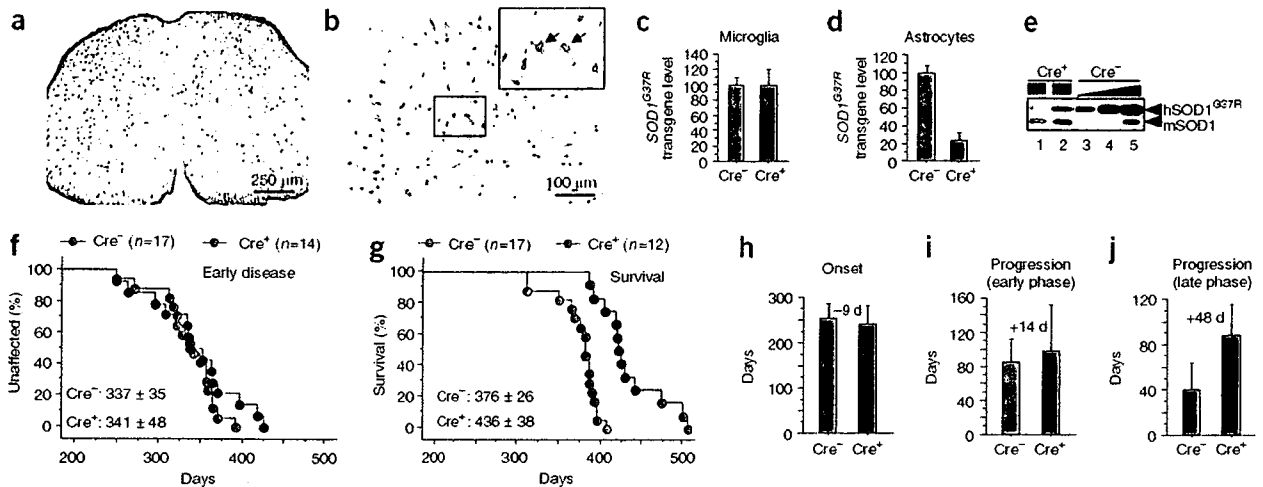


**Figure 1** Selective Cre-mediated gene excision shows that mutant SOD1 action in astrocytes is a primary determinant of late disease progression. (a,b)  $\beta$ -galactosidase ( $\beta$ -gal) activity in astrocytes in whole (a) or in the anterior horn region (b) of the lumbar spinal cord section of *GFAP-Cre/Rosa26* reporter mice visualized with X-gal and immunostaining with GFAP antibody. Inset, magnified image of the boxed area in b. Arrows indicate  $\beta$ -gal/GFAP-Cre-expressing astrocytes. (c,d) *loxSOD1<sup>G37R</sup>* transgene levels ( $n = 3$  for each group) in primary microglia (c) or astrocytes (d) from *loxSOD1<sup>G37R</sup>/GFAP-Cre<sup>+</sup>* and *loxSOD1<sup>G37R</sup>* mice using real-time PCR. (e) We determined SOD1<sup>G37R</sup> and mouse SOD1 levels by immunoblotting extracts from isolated primary astrocytes of *loxSOD1<sup>G37R</sup>/GFAP-Cre<sup>+</sup>* (lanes 1, 2) and a dilution series of a comparable extract from *LoxSOD1<sup>G37R</sup>* astrocytes representing 25%, 50% and 100% of the protein amounts loaded in lanes 1 and 2 (lanes 3–5). (f,g) Ages at which early disease phase (to 10% weight loss,  $P = 0.76$ ; f) or end-stage disease ( $P < 0.0001$ ; g) were reached for *loxSOD1<sup>G37R</sup>/GFAP-Cre<sup>+</sup>* mice (red) and *loxSOD1<sup>G37R</sup>* littermates (blue). Mean ages  $\pm$  s.d. are provided. (h–j) Mean onset ( $P = 0.47$ ) (h), mean duration of early disease (from onset to 10% weight loss,  $P = 0.35$ ; i) and a late disease (from 10% weight loss to end stage,  $P < 0.0001$ ; j) for *loxSOD1<sup>G37R</sup>/GFAP-Cre<sup>+</sup>* (red) and *loxSOD1<sup>G37R</sup>* littermates (blue). At each time point,  $P$  value was determined by unpaired  $t$ -test. Error bars denote s.d.

revealed an inverse relationship (Fig. 3a–g) between the number of astrocytes with reduced mutant SOD1 (*Cre<sup>+</sup>*) and activated microglia (correlation coefficient,  $r = -0.868$ ,  $P < 0.001$ ), despite comparable astrocytic activation. Thus, microglial activation was most prominent in areas with the highest mutant SOD1-expressing astrocyte concentration.

Elevated production of nitric oxide by upregulated inducible nitric oxide synthase (iNOS) has been reported in mutant SOD1 mice<sup>10</sup>, although deletion of the iNOS gene has modest<sup>11</sup> or no<sup>12</sup> effect on SOD1-mediated disease. It is not known in which glial cells this nitric oxide is produced in *in vivo* models of ALS, although both microglia and astrocytes have an ability to produce it when stimulated *in vitro*<sup>13</sup>. Triple staining of lumbar spinal cord sections with iNOS, Mac2 and GFAP antibodies (Fig. 3h–r) revealed that almost all iNOS-positive cells were

Mac2-positive microglia (Fig. 3n–r and Supplementary Fig. 4 online), indicating that activated microglia are the primary cell type producing nitric oxide in this SOD1 mouse model. Diminishing mutant synthesis in astrocytes inhibited iNOS induction in disease-matched, symptomatic SOD1 mice (Fig. 3h,k), consistent with substantial inhibition of microglial activation (Fig. 3i,l).

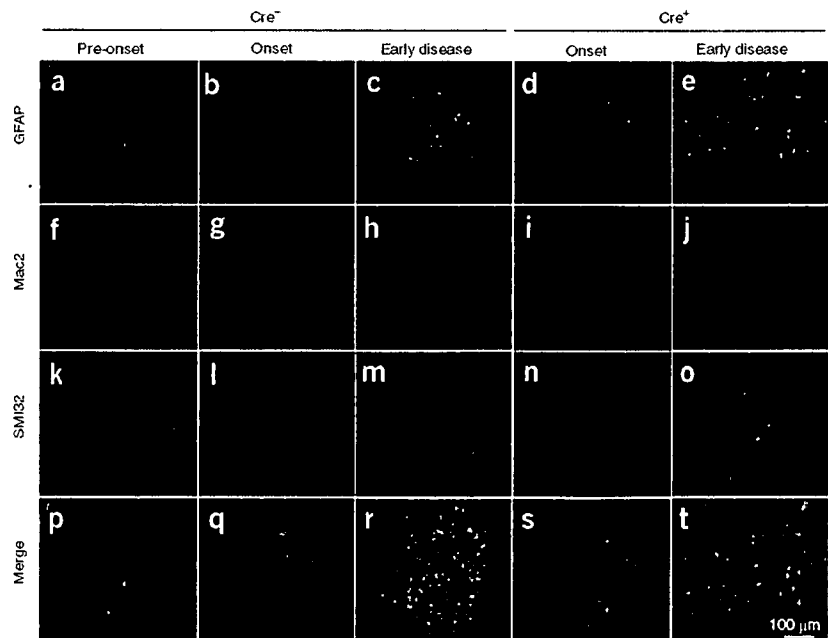


**Figure 2** Selective downregulation of mutant SOD1 in astrocytes significantly inhibits microglial activation. (a–t) GFAP-positive astrocytes (a–e), Mac2-positive activated microglia (f–j) and motor neurons identified with the neurofilament antibody SMI-32 (k–o) in the lumbar spinal cord of a *loxSOD1<sup>G37R</sup>* mouse before disease onset (a,f,k,p), at disease onset (b,g,l,q) or during early disease (c,h,m,r), together with *loxSOD1<sup>G37R</sup>/GFAP-Cre<sup>+</sup>* mice at disease onset (d,i,n,s) or during early disease (e,j,o,t). Merged images are shown in p–t.

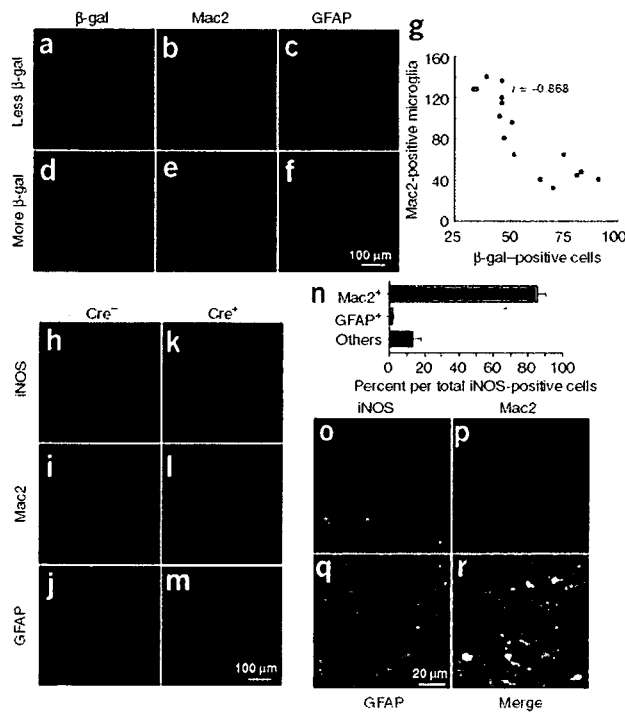


**Figure 3** Mutant-expressing astrocytes enhance microglial activation and induction of iNOS. (a–f) Images of  $\beta$ -galactosidase (a,d), Mac2 (b,e) and GFAP (c,f) staining from a left (a–c) and right (d–f) lumbar spinal cord section from a 12-month-old *loxSOD1<sup>G37R</sup>/GFAP-Cre<sup>+</sup>* mouse. *GFAP-Cre<sup>+</sup>* astrocytes are marked by  $\beta$ -galactosidase (a,d). (g) Inverted correlation between the number of Cre-positive astrocytes and Mac2-positive microglia in *loxSOD1<sup>G37R</sup>/GFAP-Cre<sup>+</sup>* mice lumbar spinal cord sections (correlation coefficient,  $r = -0.868$ ,  $P < 0.001$ ). (h–m) Lumbar spinal cord sections from *loxSOD1<sup>G37R</sup>* (h–j) and *loxSOD1<sup>G37R</sup>/GFAP-Cre<sup>+</sup>* (k–m) mice at the early disease stage immunostained with antibodies to iNOS (h,k), Mac2 (i,l), and GFAP (j,m). (n) Quantification of iNOS-positive cells in the anterior horn from lumbar spinal cord of symptomatic *loxSOD1<sup>G37R</sup>* mice. We plotted the averaged percent of iNOS<sup>+</sup>/Mac2<sup>+</sup> (red), iNOS<sup>+</sup>/GFAP<sup>+</sup> (blue) and iNOS<sup>+</sup>/other cell type (black) per total iNOS<sup>+</sup> cells. (o–r) Magnified images of anterior horn from lumbar spinal cord of symptomatic *loxSOD1<sup>G37R</sup>* mice stained with iNOS (o), Mac2 (p) and GFAP (q). Merged image illustrates that iNOS-positive cells are Mac2-positive microglia (r).

in ALS by supplementing healthy astrocytes or modulating toxicity in astrocytes to control an inflammatory response of microglia.

*Note:* Supplementary information is available on the Nature Neuroscience website.

#### ACKNOWLEDGMENTS

This work was supported by a US National Institutes of Health grant (NS 27036) and a grant from the Packard ALS Center at Johns Hopkins (D.W.C.), as well as a Muscular Dystrophy Association developmental grant, the Uehara Memorial Foundation, the Nakabayashi Trust for ALS Research and a grant-in-aid for Scientific Research (19591021) and on Priority Area (19044048) from the Ministry of Education, Culture, Sports, Science and Technology of Japan (K.Y.). Salary support for D.W.C. is provided by the Ludwig Institute for Cancer Research. S.B. is a recipient of a Fondation pour la Recherche Médicale fellowship, an Institut National de la santé et de la Recherche Médicale fellowship and a Muscular Dystrophy Association developmental grant.

#### AUTHOR CONTRIBUTIONS

K.Y., S.J.C., S.B., N.F.-T. and H.Y. conducted the experiments. D.H.G., R.T. and H.M. provided essential experimental tools and advice. K.Y., S.B., and D.W.C. were responsible for the overall design of the project, analyses of the results and writing the manuscript.

Published online at <http://www.nature.com/natureneuroscience>

Reprints and permissions information is available online at <http://npg.nature.com/reprintsandpermissions>

A role for astrocytes in inherited ALS has been previously considered in several contexts. Mutant-expressing astrocytes produce and release one or more as yet uncharacterized components that can accelerate motor neuron death *in vitro*<sup>6,7</sup>. Focal loss of the astrocytic EAAT2 glutamate transporter in affected regions<sup>14</sup> (Supplementary Fig. 5 online) and the failure of normal glutamate uptake of *SOD1<sup>G93A</sup>* astrocytes *in vitro*<sup>15</sup> support glutamate-dependent excitotoxicity as a component of disease. Nevertheless, diminished mutant *SOD1* synthesis in most astrocytes did not affect disease-dependent loss of EAAT2 from those astrocytes (Supplementary Fig. 5), indicating that a reduction in glutamate transport reflects non-cell autonomous damage to astrocytes, in part, from mutant *SOD1* synthesized by other cells. Our use of selective gene excision has now demonstrated that mutant *SOD1* damage in both microglia<sup>3</sup> and astrocytes (Fig. 1g–j) accelerates later disease progression without affecting the initiation of motor neuron degeneration and phenotypic disease onset. Discovery that damage in astrocytes determines the timing of microglial activation and infiltration provides further evidence that, beyond any direct effect of mutant astrocytes on motor neurons, such astrocytes amplify an inflammatory response from microglia (including enhanced production of nitric oxide and possibly of toxic cytokines), leading to further damage to the motor neurons and accelerated disease progression through a non-cell autonomous mechanism (Supplementary Fig. 6 online). These findings validate therapies, including astrocytic stem cell-replacement approaches, that aim to slow disease progression

1. Pasinelli, P. & Brown, R.H. *Nat. Rev. Neurosci.* **7**, 710–723 (2006).
2. Boillee, S., Vande Velde, C. & Cleveland, D.W. *Neuron* **52**, 39–59 (2006).
3. Boillee, S. *et al. Science* **312**, 1389–1392 (2006).
4. Clement, A.M. *et al. Science* **302**, 113–117 (2003).
5. Beers, D.R. *et al. Proc. Natl. Acad. Sci. USA* **103**, 16021–16026 (2006).
6. Di Giorgio, F.P., Carrasco, M.A., Siao, M.C., Maniatis, T. & Eggan, K. *Nat. Neurosci.* **10**, 608–614 (2007).
7. Nagai, M. *et al. Nat. Neurosci.* **10**, 615–622 (2007).
8. Bajenaru, M.L. *et al. Mol. Cell. Biol.* **22**, 5100–5113 (2002).
9. Fraser, M.M. *et al. Cancer Res.* **64**, 7773–7779 (2004).
10. Almer, G., Vukosavic, S., Romero, N. & Przedborski, S. *J. Neurochem.* **72**, 2415–2425 (1999).
11. Martin, L.J. *et al. J. Comp. Neurol.* **500**, 20–46 (2007).
12. Son, M., Fathallah-Shaykh, H.M. & Elliott, J.L. *Ann. Neurol.* **50**, 273 (2001).
13. Barbeito, L.H. *et al. Brain Res. Brain Res. Rev.* **47**, 263–274 (2004).
14. Howland, D.S. *et al. Proc. Natl. Acad. Sci. USA* **99**, 1604–1609 (2002).
15. Vermeiren, C. *et al. J. Neurochem.* **96**, 719–731 (2006).

## Parkin Potentiates ATP-Induced Currents Due to Activation of P2X Receptors in PC12 Cells

AYUMI SATO,<sup>1</sup> YUKIKO ARIMURA,<sup>1</sup> YOSHIMASA MANAGO,<sup>1</sup> KAORI NISHIKAWA,<sup>2</sup> KUMIKO AOKI,<sup>2</sup> ETSUKO WADA,<sup>2</sup> YASUYUKI SUZUKI,<sup>2</sup> HITOSHI OSAKA,<sup>2,3</sup> RIEKO SETSUIE,<sup>1,2</sup> MIKAKO SAKURAI,<sup>1,2</sup> TAIJU AMANO,<sup>1,2</sup> SHUNSUKE AOKI,<sup>2,4</sup> KEIJI WADA,<sup>2</sup> AND MAMI NODA<sup>1\*</sup>

<sup>1</sup>Laboratory of Pathophysiology, Graduate School of Pharmaceutical Sciences, Kyushu University, Fukuoka, Japan

<sup>2</sup>Department of Degenerative Neurological Diseases, National Institute of Neuroscience, National Center of Neurology and Psychiatry, Tokyo, Japan

<sup>3</sup>Information and Cellular Function, PRESTO, Japan Science and Technology Corporation (JST), Kawaguchi, Saitama, Japan

<sup>4</sup>NEDO (New Energy and Industrial Technology Development Organization), Kawasaki, Kanagawa, Japan

Loss-of-function mutations of the parkin gene causes an autosomal recessive juvenile-onset form of Parkinson's disease (AR-JP). Parkin was shown to function as a RING-type E3 ubiquitin protein ligase. However, the function of parkin in neuronal cells remains elusive. Here, we show that expression of parkin-potentiated adenosine triphosphate (ATP)-induced currents that result from activation of the P2X receptors which are widely distributed in the brain and involved in neurotransmission. ATP-induced inward currents were measured in mock-, wild-type or mutant (T415N)-parkin-transfected PC12 cells under the conventional whole-cell patch clamp configuration. The amplitude of ATP-induced currents was significantly greater in wild-type parkin-transfected cells. However, the immunocytochemical study showed no apparent increase in the number of P2X receptors or in ubiquitin levels. The increased currents were attenuated by inhibition of cAMP-dependent protein kinase (PKA) but not protein kinase C (PKC) or Ca<sup>2+</sup> and calmodulin-dependent protein kinase (CaMKII). ATP-induced currents were also regulated by phosphatases and cyclin-dependent protein kinase 5 (CDK5) via dopamine and cyclic AMP-regulated phosphoprotein (DARPP-32), though the phosphorylation at Thr-34 and Thr-75 were unchanged or rather attenuated. We also tried to investigate the effect of  $\alpha$ -synuclein, a substrate of parkin and also forming Lysine 63-linked multiubiquitin chains. Expression of  $\alpha$ -synuclein did not affect the amplitude of ATP-induced currents. Our finding provides the evidence for a relationship between parkin and a neurotransmitter receptor, suggesting that parkin may play an important role in synaptic activity. *J. Cell. Physiol.* 209: 172–182, 2006. © 2006 Wiley-Liss, Inc.

Recessive juvenile-onset form of Parkinson's disease (AR-JP) is the most frequent form of familial Parkinson's disease (PD). Mutations in the parkin gene were originally discovered from the linkage study of Japanese AR-JP families (Kitada et al., 1998). Thereafter its mutations have been found worldwide and parkin gene is now accepted as one of eight genes responsible for Parkinson's disease (see review by Cookson, 2005).

It has been demonstrated that parkin is associated with the ubiquitin–proteasome system. Wild-type parkin encodes for a protein-ubiquitin E3 ligase, which ubiquitinates many substrate proteins to enhance their degradation by the 26S proteasomes (Imai et al., 2000; Shimura et al., 2000; Zhang et al., 2000). As parkin mutations lose their E3 ligase activity, it is thought that accumulation of parkin substrate may lead to the selective death of catecholaminergic cell death (Ko et al., 2005) and familial-associated mutations differentially disrupt the solubility, localization, binding, and ubiquitination properties of parkin (Sriram et al., 2005).

It is reported that parkin is localized on surface of synaptic vesicle membranes (Kubo et al., 2001). As substrates of parkin, some synaptic proteins were reported, such as synaptotagmin XI (Huynh et al., 2003), septin CDCrel-1 (Zhang et al., 2000), and synphylin1 (Lim et al., 2005), suggesting that parkin may have a neuronal function. However, the nature of this function is unknown. Therefore, we have investigated the effect of parkin on one of receptor channels that affect neurotransmitter secretion.

Adenosine triphosphate (ATP) and related nucleotides induce a release of catecholamines, including dopamine, in PC12 pheochromocytoma cells, a frequently used model for sympathetic neurons (Sela et al., 1991; Nakazawa and Inoue, 1992). ATP receptors are divided into two subtypes, P2X and P2Y receptors.

Ayumi Sato and Yukiko Arimura contributed equally to this work.

Contract grant sponsor: Japan Society for Promotion of Science; Contract grant number: 15082214; Contract grant sponsor: Ministry of Education, Culture, Sports, Science and Technology, Japan; Contract grant number: 16300126; Contract grant sponsor: Ministry of Health, Labour and Welfare, Japan; Contract grant sponsor: National Institute of Biomedical Innovation (NIBIO) Japan; Contract grant number: 05-32.

Yoshimasa Manago's present address is Foods and Fine Chemicals Department, Products Development Section, Maruha Corporation, Tochigi 321-3231, Japan.

Hitoshi Osaka's present address is Division of Neurology, Clinical Research Institute, Kanagawa, Children's Medical Center, Yokohama, 232-8555, Japan.

\*Correspondence to: Mami Noda, Laboratory of Pathophysiology, Graduate School of Pharmaceutical Sciences, Kyushu University, 3-1-1 Maidashi, Higashi-ku, Fukuoka 812-8582, Japan. E-mail: noda@phar.kyushu-u.ac.jp

Received 8 October 2005; Accepted 5 June 2006

DOI: 10.1002/jcp.20719

P2X receptors are ionotropic receptors and form cationic channels, while P2Y receptors are G-protein-coupled receptors. Recently, we have reported that P2X receptor-induced membrane currents were augmented by ubiquitin carboxy-terminal hydrolase L1 (UCH-L1), presumably due to upregulation of mono-ubiquitin level (Manago et al., 2005). Therefore, the ubiquitin-proteasome pathway is also implicated in the function of ATP receptors.

In the present study, we analyzed relationships between parkin and P2X receptors by expressing parkin or a familial-linked mutant parkin (T415N-parkin) which lacks ubiquitin E3 ligase activity in PC12 cells. This is the first evidence to show the relationship between physiological function of parkin and receptor channels involved in neurotransmitter secretion. These findings may help to understand the function of parkin in the nervous system and the mechanism of Parkinson's disease caused by dysfunction of parkin.

## MATERIALS AND METHODS

### Chemicals

RPMI-1640 medium, ATP-2Na, H-89 (N-[2-(p-bromoocina-mylamino)ethyl]-5-isoquinolinesulfonamide), H-85, chelerythrine, roscovitine (2-(R)-(1-Ethyl-2-hydroxyethylamino)-6-benzylamino-9-isopropylpurine), and PD98059 (2'-Amino-3'-methoxyflavone) were from Sigma (St. Louis, MO). Nerve growth factor (NGF) and Lipofectamine 2000 were from Invitrogen (Carlsbad, CA). KN-93 (2-[N-(2-hydroxyethyl)]-N-(4-methoxybenzenesulfonyl)amino-N-(4-chlorocinnamyl)-N-methylbenzylamine) and okadaic acid was from Calbiochem (San Diego, CA).

### Cell culture

PC12 Tet-off cells were grown in RPMI-1640 medium containing 5% fetal bovine serum (FBS) (Cell Culture Technologies, Lugano, Switzerland), 10% horse serum (HS) (Invitrogen), 100 units/ml penicillin (Life Technologies, Rockville, MD), and 100 µg/ml streptomycin (Life Technologies) in a humidified atmosphere with 10% CO<sub>2</sub> at 37°C. To differentiate cells, 100 ng/ml of NGF was added to the RPM 1640 medium with 0.1% HS, 0.05% FBS, 50 unit/ml penicillin, and 100 µg/ml streptomycin for 4 days.

### Transfection

Plasmids used for transfection were constructed using pIRES-EYFP vector (Clontech, Nottinghamshire, UK). For electrophysiological recording, PC12 Tet-Off cells were transfected with mock, Flag-tagged wild-type or mutant (T415N) parkin cDNA, using Lipofectamine 2000. The engineered PC12 cells are constructed to have higher transfection efficiency than wild-type PC12 cells (unpublished data). After 24 h of transfection, cells were treated with NGF and differentiated for 4–5 days. More precisely,  $3.0 \times 10^5$  cells were seeded in 35-mm dishes in RPMI with 10% HS and 5% FBS. Twenty-four hours after seeding, the medium was replaced with 500 µl of serum-free RPMI 1640 medium. Then, the transfection mixture containing 4 µg of cDNA and 10 µl of Lipofectamine 2000 in 500 µl of RPMI-1640 was added to each dish and incubated for 6 h in a humidified atmosphere with 10% CO<sub>2</sub> at 37°C. One milliliter of complete RPMI-1640 supplemented with an additional 10% HS and 5% FBS was then added to each dish. The solution for transfection was discarded 18 h later and replaced with RPMI-1640 medium for differentiation with added 100 ng/ml NGF. For transfection of  $\alpha$ -synuclein, plasmids were constructed using pIRES-EGFP vector (Clontech) and the same protocol was used as for parkin. For protein analysis, cells ( $7.5 \times 10^5$ /well, Clontech) were transfected in the same way. After 24 h, cells were subjected to Western blot analysis.

### Western blot analysis

After 48 h of transfection of pIRES-EYFP-mock, pIRES-EYFP-Flag-wild-type parkin, or T415N parkin with Lipofec-

tamine 2000 (Invitrogen), cells were lysed with TBS buffer (25 mM Tris/150 mM NaCl, PH 7.4) containing 1% Triton X-100 and centrifuged at 15,000 rpm for 30 min at 4°C. Thirty micrograms of each protein was subjected to SDS-PAGE on a 15% gel and transferred to PVDF membranes (Bio Rad, CA) and immunoblotted with anti-Flag M2 (1:200, Sigma, monoclonal) or anti-Actin (1:200, Chemicon, Temecula, CA, monoclonal).

### Immunocytochemical analysis

After transfection, cells were fixed with 4% paraformaldehyde. Immunocytochemistry on PC12 Tet-Off cells was performed as previously described (Osaka et al., 2003) using antibodies against parkin (5 µg/ml, Zymed, San Francisco, CA; monoclonal), P2X<sub>2</sub>, P2X<sub>4</sub>, or P2X<sub>6</sub> receptor (1:200, Alomone labs, Jerusalem, Israel; polyclonal), ubiquitin that is predominantly reactive to free ubiquitin in immunohistochemistry (1:100, Sigma; polyclonal),  $\alpha$ -synuclein (1:500, BD Biosciences, San Jose, CA), and dopamine and cyclic AMP-regulated phosphoprotein (DARPP-32) (phosphor Thr-34 and phospho Thr-75) (1:500, Abcam, Cambridge, UK). For immunofluorescence studies, anti-rabbit IgG conjugated with Cy3 antibodies (1:200, Jackson Immuno Research, West Grove, PA) or Alexa Fluor 568 goat anti-mouse (1:250, Molecular Probes, Invitrogen) was used as secondary antibodies. The same strength of the laser wavelength or fluorescence was applied in the series of images, for the quantification of the fluorescence under the confocal laser microscope system (LSM510, Carl Zeiss, Oberkochen, Germany).

### Electrophysiological measurements

Cells expressing EYFP were selected under the fluorescence microscope. A patch pipette was then applied to the cell to obtain a giga-ohm seal under phase-bright mode. Whole-cell membrane current recordings were made under voltage-clamp at a holding potential of -70 mV as reported previously (Noda et al., 2000; Manago et al., 2005), using an Axopatch-200B amplifier (Axon Instruments, Foster City, CA). The patch pipette was filled with a solution containing (in mM): CsCl, 120; Mg<sub>2</sub>ATP<sub>3</sub>, 3; HEPES, 20; CaCl<sub>2</sub>, 1; MgCl<sub>2</sub>, 1; EGTA, 5. The pH of the solution was adjusted to 7.2 with 1 N CsOH. The pipette resistance was 5–9 M $\Omega$ . The external solution contained (mM): NaCl, 132; KCl, 5; CaCl<sub>2</sub>, 2; MgCl<sub>2</sub>, 1; glucose, 10; and HEPES, 10. The pH was adjusted to 7.4 with 1 N NaOH. External ATP or drugs were applied rapidly using the 'Y tube' technique (Min et al., 1996), which allows the complete exchange of the external solution surrounding a cell within 20 msec. Temperature monitored in the recording dishes was 33–34°C.

In the experiments using inhibitors (except PD98059), ATP was applied twice to ensure reproducibility of the ATP-induced current in control experiments. The inhibitor solution was applied after first application of ATP for a period appropriate to the inhibitor until the end of second application of ATP. The current amplitude obtained at the second application of ATP with or without inhibitors was normalized to that of the first ATP-induced current. All values were presented as mean  $\pm$  SEM. Statistical analysis was done using ANOVA. A value of  $P < 0.05$  was considered to be the minimum level of significance. Curve fitting was performed using the standard Hill Equation (Igor Pro 4.07; Wavemetrics, Lake Oswego, OR).

## RESULTS

### Transfection of parkin in PC12 Tet-Off cells

Expression of plasmid constructs was first examined in PC12 Tet-Off cells. Western blot analysis showed immunoreactive bands by anti-Flag antibodies in cells transfected with pIRES-EYFP-wild type parkin or T415N parkin, but not with mock plasmids (Fig. 1A). The efficiency of the transfection was about 10% in PC12 Tet-Off cells. To test endogenous expression of parkin, cells were immunostained using specific antibodies for parkin. The strong expression of parkin (red) was observed in wild-type parkin-transfected cell (yellow) but not in non-transfected cells in the same field (shown

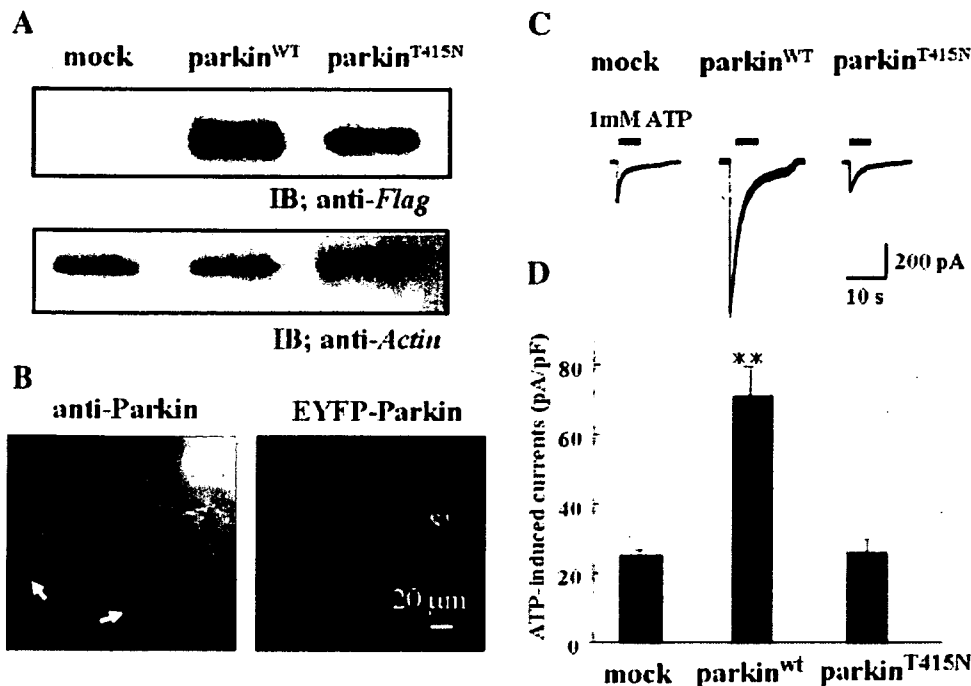


Fig. 1. Transfection of parkin and potentiation of ATP-induced currents in PC12 cells. **A:** Western blot analysis of PC12 Tet-Off cells. Cells were transfected with either pIRES-EYFP-mock, wild-type (WT) parkin, or T415N parkin. Each protein was subjected to SDS-PAGE and immunoblotted with anti-Flag or anti-Actin antibody. **B:** Confocal image of PC12 Tet-Off cells transfected with pIRES-EYFP-wild-type parkin (yellow) showed strong expression level of parkin (red) while

non-transfected cells (white arrows) showed little expression of parkin. **C:** Inward membrane currents induced by 1 mM ATP at the holding potential of  $-70$  mV in mock-, wild-type parkin-, and T415N parkin-transfected PC12 Tet-Off cells. **D:** Amplitudes of peak inward currents induced by 1 mM ATP in mock-, wild-type parkin-, and T415N parkin-transfected PC12 Tet-Off cells. The bars represent the mean  $\pm$  SEM,  $**P < 0.01$ .

with white arrows in Fig. 1B), suggesting little endogenous parkin was expressed in PC12 Tet-Off cells.

#### Effects of expression of parkin on ATP-induced currents

ATP-activated inward currents due to the activation of P2X receptors at negative holding potentials in PC12 cells or PC12 Tet-Off cells have been reported previously (Nakazawa et al., 1994; Manago et al., 2005). In our experiments, PC12 Tet-Off cells were voltage-clamped at  $-70$  mV and 1 mM ATP were applied to see whether or not overexpression of parkin affected maximum inward currents. In parkin-transfected cells, ATP-induced inward currents were nearly threefold larger than those in mock- or mutant (T415N) parkin-transfected cells (Fig. 1C). The amplitudes of the peak inward currents in mock-, wild-type parkin-, and T415N parkin-transfected PC12 Tet-Off cells were  $24.8 \pm 1.6$  pA/pF ( $n = 9$ ),  $71.3 \pm 8.4$  pA/pF ( $n = 5$ ), and  $26.1 \pm 3.4$  pA/pF ( $n = 7$ ), respectively (Fig. 1D).

The current-voltage relationships of the ATP-induced inward currents were determined by applying 50 msec voltage steps in 10 mV increments between  $-100$  mV and  $+50$  mV at 50 msec interval from the holding potential of  $-70$  mV before and during the application of ATP (Fig. 2A). Current traces obtained before and after application of ATP in wild-type parkin-transfected cells are shown in Figure 2B. The current levels at the end of each pulse before and during ATP application were measured in mock-, wild-type parkin-, or T415N parkin-transfected cells. The amplitudes of the ATP-induced currents at each voltage were obtained by subtracting the one before application of ATP from the one during application of ATP. The current-voltage relationships obtained at the time point after 40 msec from the beginning of each pulse were plotted as in

Figure 2C. To allow for possible desensitization, the current-voltage relationships were also obtained by applying voltage steps in the opposite direction, that is, from  $+50$  to  $-100$  mV, but there was little change (data not shown). The reversal potential was about 0 mV, suggesting that these currents were due to non-specific cationic channels.

ATP-induced inward currents were concentration-dependent. Mock- and T415N parkin-transfected cells showed visible ATP-induced inward currents at 0.03 nM and a maximum response at 1 mM ATP (Fig. 3A). The maximum response was almost three times bigger in wild-type parkin-transfected cells (Fig. 3B). The sensitivity to ATP was not significantly changed by overexpression of either mock, wild-type, or T415N parkin.  $EC_{50}$  values (half maximum concentration) were  $187 \pm 45$   $\mu$ M,  $127 \pm 13$   $\mu$ M, and  $177 \pm 124$   $\mu$ M with Hill coefficients ( $n_H$ ) of  $1.05 \pm 0.314$ ,  $0.97 \pm 0.12$ , and  $2.00 \pm 2.26$  in mock-, wild-type, and T415N parkin-transfected cells, respectively.

#### Expression of P2X<sub>2</sub>, P2X<sub>4</sub>, and P2X<sub>6</sub> receptors in parkin-transfected cells

In PC12 cells, P2X<sub>2</sub> and P2X<sub>4</sub> receptors (Hur et al., 2001) with lower level of P2X<sub>6</sub> receptor are expressed (our unpublished data). It was possible that the expression of P2X receptors was enhanced by overexpression of parkin. To define the changes in the expression level of P2X receptors semi-quantitatively, P2X<sub>2</sub>, P2X<sub>4</sub>, and P2X<sub>6</sub> receptors were immunostained using specific antibodies for each receptor subtype. The subcellular localization of P2X<sub>2</sub>, P2X<sub>4</sub>, and P2X<sub>6</sub> receptors showed no obvious difference in wild-type parkin-transfected cells compared with non-transfected cells in the same field (Fig. 4), suggesting that the potentiation of the



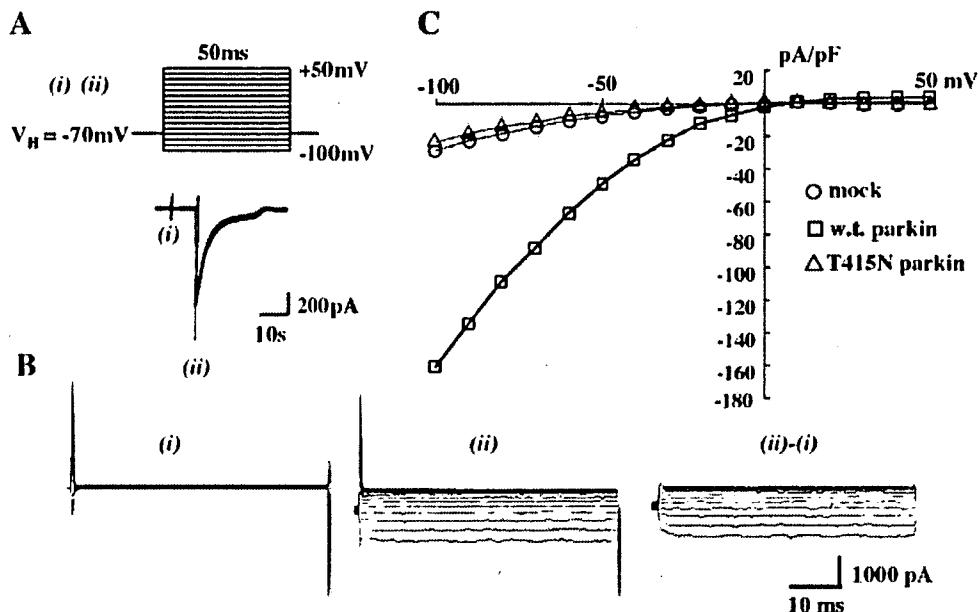


Fig. 2. Voltage-dependency of ATP-induced currents in mock-, wild-type parkin-, and T415N parkin-transfected PC12 Tet-Off cells. A: The voltage protocol shown in the upper part was applied before and during application of 1 mM ATP at the time indicated by (i) and (ii) in the lower part. B: Cumulated current traces obtained in wild-type parkin-transfected cells before (i) and during (ii) application of ATP.

The subtracted currents [(ii) – (i)] show the ATP-induced currents. C: The current–voltage relationships of ATP-induced currents. The amplitudes of subtracted currents [(ii) – (i)] in (B) at the end of 50 msec pulses were plotted against the pulse potentials in mock (○)-, wild-type (w.t.) parkin (□)-, and T415N parkin (△)-transfected cells.

ATP-induced currents was not due to an increase in the total number of P2X receptors.

**Expression of mono-ubiquitin in parkin-transfected cells**

It has previously been reported that a de-ubiquitinating isozyme, ubiquitin carboxy-terminal hydrolase L1 (UCH-L1), also potentiated ATP-induced currents (Manago et al., 2005). However, hydrolase activity was not involved in the potentiation of ATP-induced currents because a mutant form lacking hydrolase activity also potentiated the current. Instead, UCH-L1 upregulated ubiquitin levels (Osaka et al., 2003) and over-expression of UCH-L1 in PC12 cells increased the mono-

ubiquitin level (Manago et al., 2005). To test whether or not parkin also upregulate mono-ubiquitin levels, ubiquitin was stained using anti-mono-ubiquitin IgG. Unlike the effect of UCH-L1, immunoreactivity for ubiquitin in wild-type parkin-transfected cells was unchanged compared to that in mock-transfected cells or non-transfected cells in the same field (Fig. 5). These results indicated that parkin did not upregulate mono-ubiquitin.

**Little effects of  $\alpha$ -synuclein on ATP-induced currents**

Since it has recently been shown that UCH-L1, parkin, and  $\alpha$ -synuclein form lysine 63-linked multi-ubiquitin chains (Doss-Pepe et al., 2005; Lim et al.,

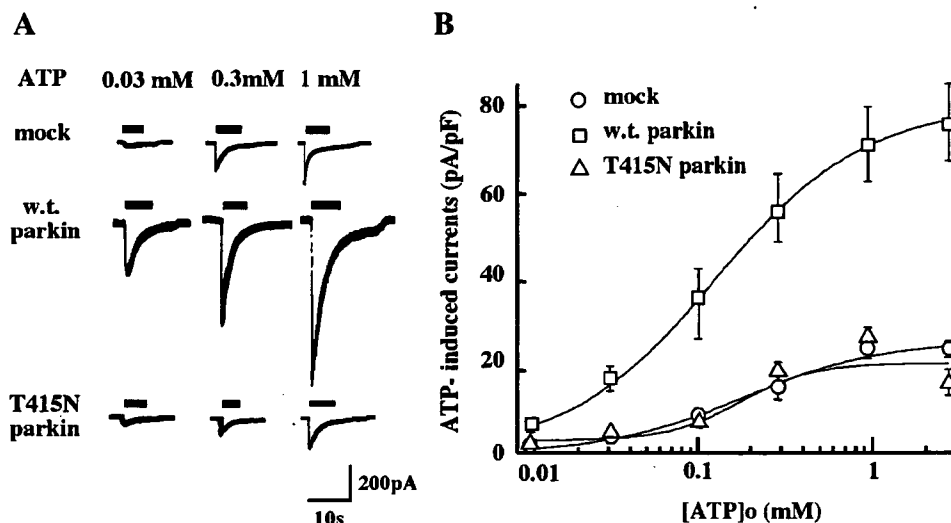


Fig. 3. Concentration-dependent curve of ATP-induced currents in mock-, wild-type parkin-, and T415N parkin-transfected PC12 Tet-Off cells. A: Inward membrane currents induced by 0.03, 0.1, and 1 mM ATP at the holding potential of  $-70$  mV in mock-, wild-type (w.t.) parkin-, and T415N parkin-transfected PC12 Tet-Off cells. B: The peak inward current induced by ATP at the holding potential of

$-70$  mV was plotted against the ATP concentration at several points between 0.01 and 3 mM in the mock (○)-, wild-type parkin (□)-, and T415N parkin (△)-transfected PC12 Tet-Off cells. Each point represents the mean of 5–13 cells and the bar shows the mean  $\pm$  SEM. The curve shows the least squares fit.

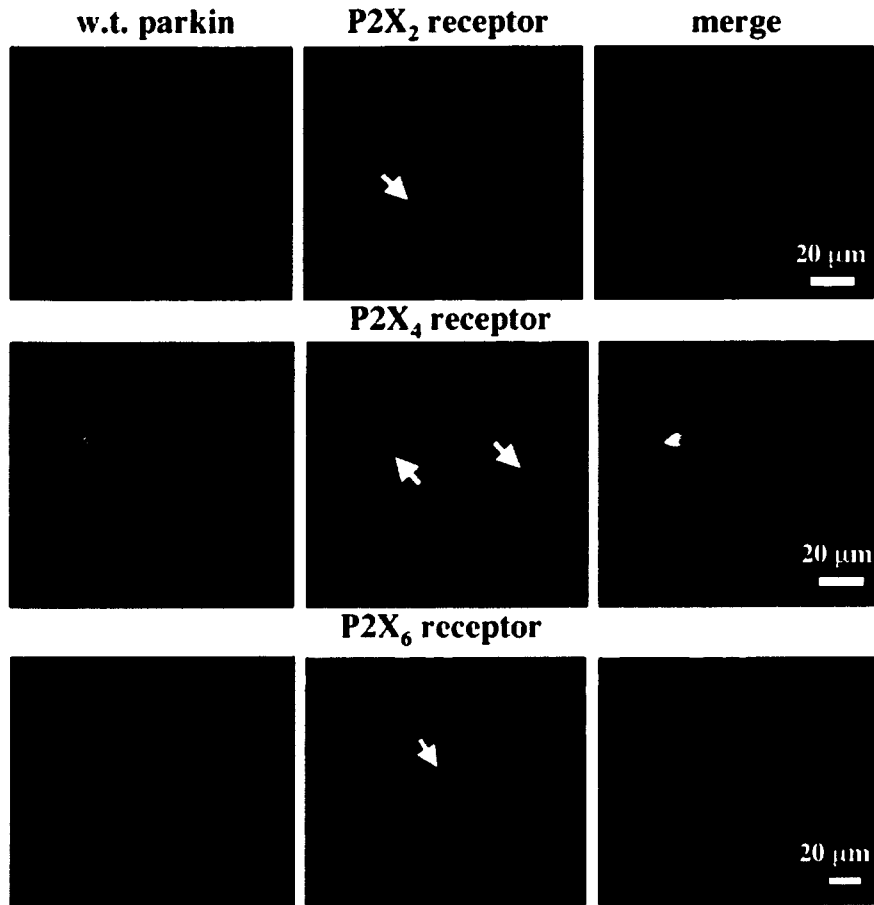


Fig. 4. Parkin has no clear effect on the expression of P2X<sub>2</sub>, P2X<sub>4</sub>, and P2X<sub>6</sub> receptors. Confocal images of PC12 Tet-Off cells transfected with pIRES-EYFP-wild-type (w.t.) parkin that were double stained with P2X<sub>2</sub> (upper part), P2X<sub>4</sub> (middle part), and P2X<sub>6</sub> receptors (lower part). EYFP (yellow)-positive cells were parkin-transfected cells, showing similar expression level of P2X receptors (red) to those in non-transfected cells.

2005),  $\alpha$ -synuclein also might have a similar effect on P2X receptor. Transfection of  $\alpha$ -synuclein was performed in the same way as parkin and the transfection efficiency was much greater than that of parkin (up to

30%) and the protein expression was confirmed by Western blotting (not shown). The strong expression of  $\alpha$ -synuclein (red) was observed in transfected cell (green) but not in non-transfected cells in the same field

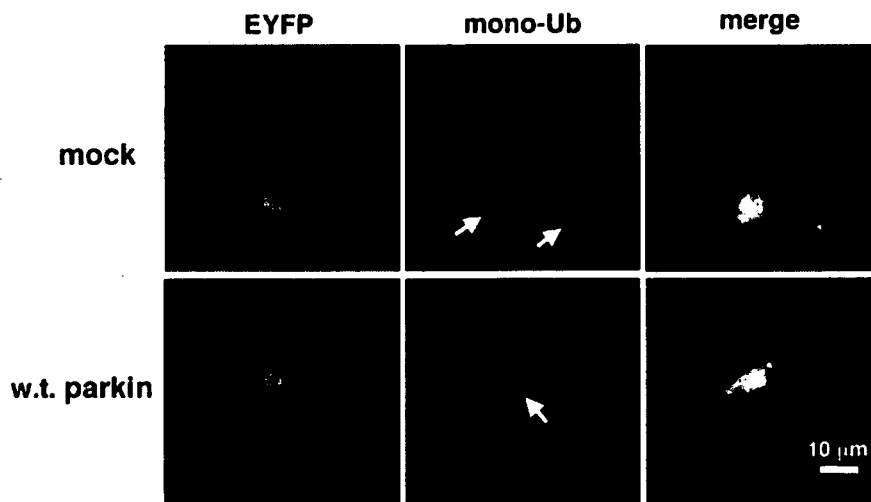


Fig. 5. Parkin had no clear effect on mono-ubiquitin expression. Confocal images of PC12 cells transfected with pIRES-mock or wild-type (w.t.) parkin that were double stained with mono-ubiquitin (red) and EYFP (yellow).

(shown with white arrows in Fig. 6A), suggesting little endogenous  $\alpha$ -synuclein was expressed in PC12 Tet-Off cells.

ATP-induced currents in  $\alpha$ -synuclein-transfected cells were not significantly different from those in mock-transfected cells (Fig. 6B). The relative amplitude of ATP-induced currents were  $28.6 \pm 4.1$  pA/pF ( $n = 9$ ) in mock-transfected cells and  $21.5 \pm 5.4$  pA/pF ( $n = 10$ ) in  $\alpha$ -synuclein-transfected cells, respectively.

#### Effects of kinase inhibitors on ATP-induced currents in parkin-transfected cells

The mechanism by which ATP-induced currents were augmented in parkin-transfected cells was investigated. It was reported that in *Aplysia* UCH activated PKA as a result of degradation of the regulatory subunit of PKA, and that this contributed to the long-term potentiation (Hegde et al., 1997). The increase of the ATP-induced inward currents in UCH-L1-transfected cells has also been attributed to activation of PKA (Manago et al., 2005). Therefore, it was tested whether PKA might be activated in parkin-transfected cells by using H-89, a PKA inhibitor. After obtaining large ATP-induced currents in parkin-transfected cells, 10  $\mu$ M H-89 was applied for 10 min. The amplitude of the ATP-induced currents in the presence of H-89 was  $64.6 \pm 3.5\%$  ( $n = 7$ ) of that of the first ATP-induced current in the same cell (control without H-89;  $85.3 \pm 4.0\%$  ( $n = 4$ )) (Fig. 7A), implying an inhibition of about 25%. An inactive analog of H-89, H-85, did not have this inhibitory effect (current amplitude in the presence of H-85 was  $84.3 \pm 1.6\%$  ( $n = 3$ ) of the first current). To confirm the effect of parkin, the effect of PKA inhibitor on ATP-induced currents were tested in mock-transfected cells as well. In mock-transfected cells, application of 10  $\mu$ M H-89 for 10 min had no effect on the ATP-induced inward current (H-89,  $79.8 \pm 1.4\%$  ( $n = 3$ ); control;  $77.6 \pm 5.2\%$  ( $n = 3$ )) (Fig. 7B).

The intracellular carboxyl terminus of P2X receptor contains several consensus phosphorylation sites for protein kinase C (PKC) as well as PKA, suggesting that the function of the P2X receptors might be regulated by PKC-mediated phosphorylation (Chow and Wang, 1998). Hence, the effect of chelerythrine, a PKC inhibitor, on ATP-induced currents in parkin-transfected

cells was tested. Application of 5  $\mu$ M chelerythrine for 10 min had no effect on the ATP-induced inward current in wild-type parkin-transfected cells (Fig. 7A). The normalized amplitude of second ATP-induced inward currents in the presence of chelerythrine was  $88.4 \pm 3.3\%$  ( $n = 5$ ). The possible involvement of calmodulin-dependent protein kinase (CaMKII) was also tested by using KN-93, a CaMKII inhibitor. Application of 10  $\mu$ M KN-93 for 20 min had no effect on the ATP-induced inward current in wild-type parkin-transfected cell ( $90.4 \pm 5.1\%$  ( $n = 4$ ); control,  $81.2 \pm 4.6\%$  ( $n = 4$ )) (Fig. 7C).

In PC12 cells and hippocampal neurons, activation of PKA has been reported to cause activation of extracellular signal-regulated kinase (ERK), with subsequent phosphorylation of  $\text{Ca}^{2+}$ -stimulated cAMP response element binding protein (CREB) and stimulated transcription (Impey et al., 1998). Likewise, the augmentation of ATP response in parkin-transfected cell might be due to the stimulation of transcription. To test this possibility, we examined whether mitogen-activated protein kinase (MAPK), including ERK, was activated following the activation of PKA in PC12 Tet-Off cells. However, ATP-induced currents in parkin-transfected cells were unaffected even after application of 5  $\mu$ M PD98059, (one of the MAPK kinase inhibitors) for 4 days: the amplitude of the ATP-induced current after the application of PD98059 was  $82.1 \pm 9.9$  pA/pF ( $n = 4$ ) compared with  $74.6 \pm 3.4$  pA/pF ( $n = 18$ ) in controls treated with vehicle (Fig. 7D).

#### Involvement of DARPP-32 in parkin-transfected PC12 Tet-Off cells

It was previously reported that the dopamine and cAMP-regulated phosphoprotein with molecular weight of about 32,000 (DARPP-32) was expressed in PC12 Tet-Off cells and that the expression level tended to increase after differentiation of the cells with NGF (Manago et al., 2005). Since phosphorylation of DARPP-32 at Thr-75 by cyclin-dependent kinase 5 (CDK5) had a negative feedback regulatory effect on PKA activity (Nishi et al., 2000), the effect of roscovitine, a CDK5 inhibitor, was tested. The application of 10  $\mu$ M roscovitine to wild-type parkin-expressing cells for 10 min enhanced the normalized amplitude of ATP-induced currents to the one

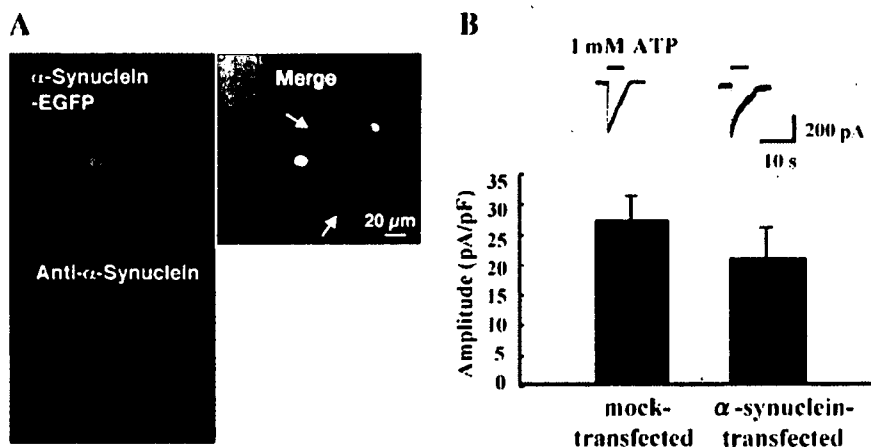


Fig. 6. The wild-type  $\alpha$ -synuclein-transfection had no effect on ATP-induced currents. A:  $\alpha$ -synuclein-transfected cells (EGFP; green) were strongly stained with anti- $\alpha$ -synuclein (red), while non-transfected cells (with arrows) were not. B: The amplitude of ATP-induced inward currents in mock and  $\alpha$ -synuclein-transfected cells.

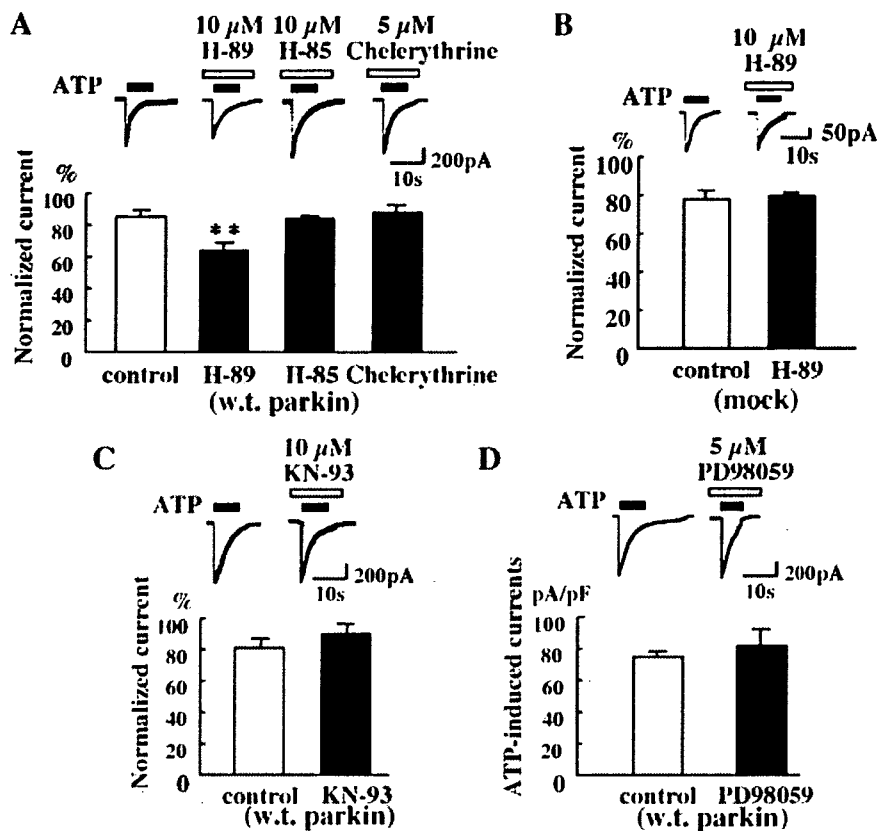


Fig. 7. Effects of kinase inhibitors on ATP-induced currents. A: In wild-type parkin-transfected cells, ATP-induced currents were attenuated by pre-application of 10  $\mu$ M H-89, a PKA inhibitor, but not either by 10  $\mu$ M H-85, an inactive analog of H-89, or 5  $\mu$ M chelerythrine, a PKC inhibitor, for 10 min. B: H-89 had no effect on

ATP-currents in control (mock-transfected) cells. C, D: In wild-type parkin-transfected cells, ATP-induced currents were not affected by application of 10  $\mu$ M KN-93, a CaMKII inhibitor, for 20 min (C), or by treatment with 5  $\mu$ M PD98059, a MAPKK inhibitor, for 4 days during differentiation (D). \*\* $P < 0.01$ .

before application of roscovitine ( $102.1 \pm 3.5\%$  ( $n = 4$ ); control without roscovitine;  $85.3 \pm 4.0\%$  ( $n = 4$ )) (Fig. 8A). The result suggested that PKA activity in parkin-transfected cells was negatively regulated by the phosphorylation of DARPP-32 at Thr-75 by CDK5.

Activation of PKA also influenced on protein phosphatases relating to DARPP-32 (Nishi et al., 2000). The phosphorylation of DARPP-32 at Thr-34 has been reported to inhibit protein phosphatase-1 (PP-1), leading to an apparent increase in substrate-phosphorylation. On the other hand, PKA activates protein phosphatase-2A (PP-2A), causing dephosphorylation of DARPP-32 at Thr-75, activating PKA in turn. To investigate the role of PP-1 and PP-2A in parkin-transfected cells, we applied 100 nM okadaic acid, an inhibitor for both PP-1 and PP-2A, for 20 min. The normalized currents were augmented to  $98.7 \pm 4.5\%$  ( $n = 5$ ) (control without okadaic acid;  $81.2 \pm 4.6\%$  ( $n = 4$ )) (Fig. 8B). These results suggested that the function of PP-1 was superior to that of PP-2A in parkin-transfected cells.

The effects of CDK5 inhibitor and okadaic acid on ATP-induced currents were tested in mock-transfected cells as well. In mock-transfected cells, application of 10  $\mu$ M roscovitine for 10 min had no effect on the ATP-induced inward current (roscovitine,  $82.5 \pm 5.2\%$  ( $n = 3$ ); control;  $77.6 \pm 5.2\%$  ( $n = 3$ )) (Fig. 8C). Similarly, application of 100 nM okadaic acid for 20 min did not affect the ATP-induced currents in mock-transfected cells, ( $76.5 \pm 3.5\%$  ( $n = 3$ ); control;  $80.0 \pm 4.7\%$  ( $n = 3$ )) (Fig. 8D).

#### Phosphorylation of DARPP-32 in parkin-transfected PC12 Tet-Off cells

To investigate whether or not the phosphorylation of DARPP-32 at Thr-34 or Thr-75 was modified by parkin, cells were immunostained using specific antibodies for DARPP-32 (phospho Thr-34 or phospho Thr-75). The staining of phospho Thr-34 in parkin-transfected cells were not enhanced as expected from the activation of PKA (Nishi et al., 2000) but rather attenuated (Fig. 9A). While phospho Thr-75 looked similar between parkin-transfected cell and non-transfected cells in the same field (Fig. 9B).

#### DISCUSSION

To understand the functional role of parkin in the central nervous system (CNS), it is important to know whether parkin has any effects on ion channels and receptors that are the basic elements of neurotransmission. To test this, we used PC12 cells and overexpressed parkin protein (Fig. 1A). These show well-developed inward current response to stimulation of P2X receptors by ATP (Nakazawa et al., 1994) and we recently reported enhancement of these currents by ubiquitin C-terminal hydrolase L1 (UCH-L1) (Manago et al., 2005). In the present experiments, we have studied the effects of overexpressing of parkin on these currents.

Parkin produced a very substantial increase in the maximum ATP-induced current without significant change in sensitivity to ATP (Figs. 1 and 3). This did not appear to be due to an increased number of P2X<sub>2</sub>,

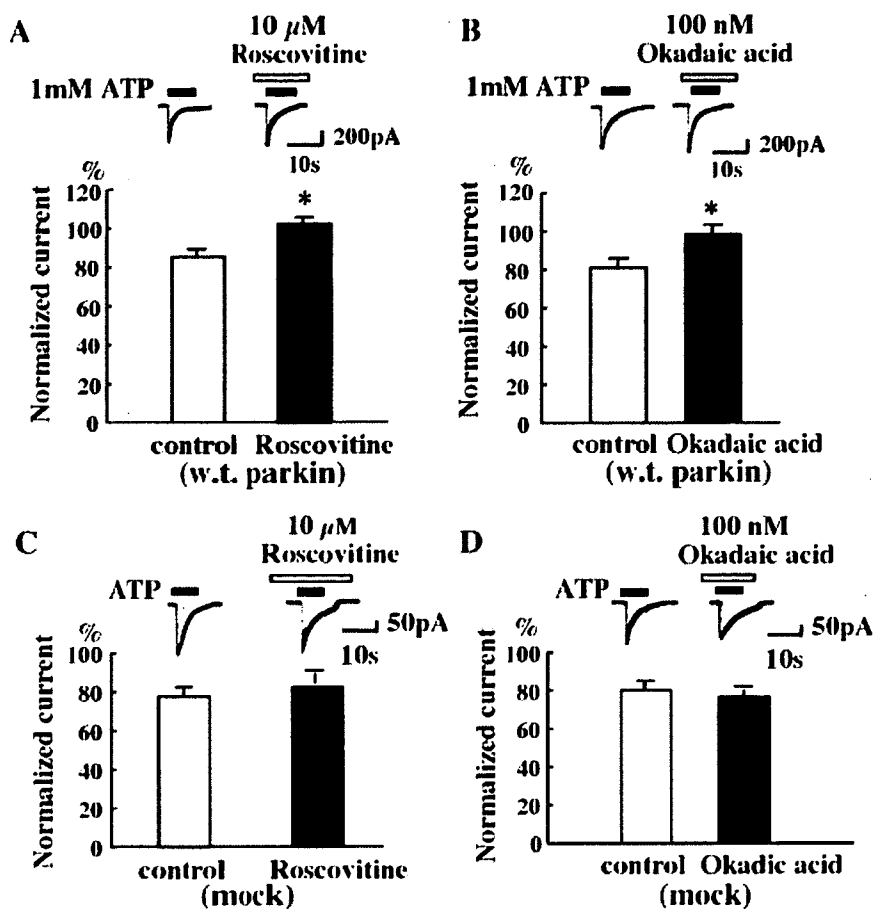


Fig. 8. Involvement of DARPP-32-related protein kinase and protein phosphatase on ATP-induced currents. In wild-type parkin-transfected cells, ATP-induced currents were augmented by pre-application of roscovitine, a CDK5 inhibitor, for 10 min (A) or 100 nM okadaic acid, a protein phosphatase inhibitor, for 20 min (B). In mock-transfected cells, ATP-induced currents were not affected by 10 μM roscovitine (C) or 100 nM okadaic acid (D). \*\**P* < 0.05.

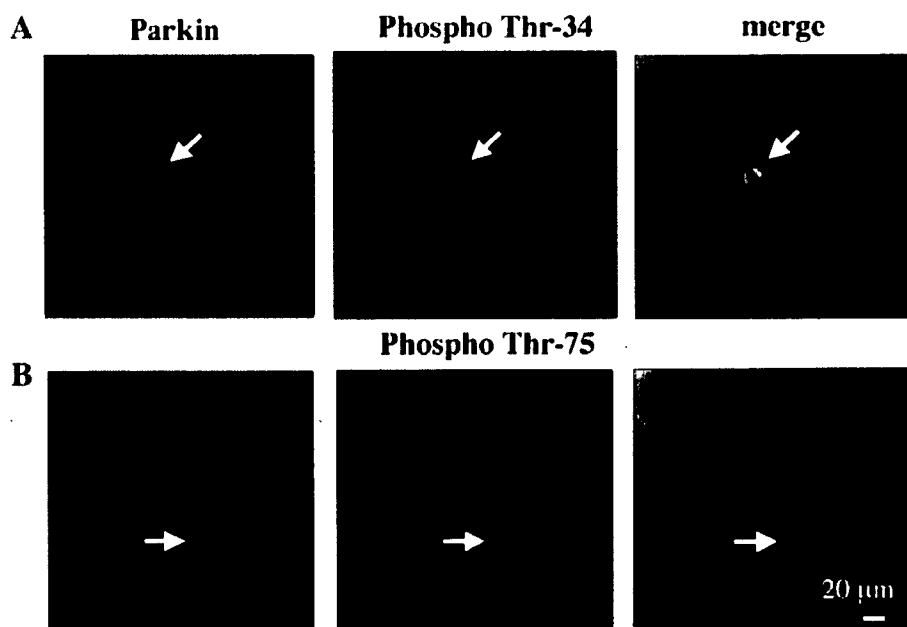


Fig. 9. Parkin did not increase the phosphorylation of DARPP-32. **A:** Immunostaining of phospho Thr-34 (red) looked rather smaller in parkin-transfected cell (yellow-green; white arrow). **B:** Immunostaining of phospho Thr-75 (red) looked similar between parkin-transfected cell (white arrow) and non-transfected cells. The merged images also include differential interference contrast images.

P2X<sub>4</sub>, or P2X<sub>6</sub> receptors, as judged by immunocytochemistry (Fig. 4). Therefore, the mechanism seems to involve an increase in gating of the receptors, rather than increased affinity or receptor number. Enhancement of P2X receptor at presynaptic terminal could increase neurotransmitter release; it was reported that ischemia-induced facilitation of glutamate release was due to the activation of P2X receptors in spiny neuron in neostriatum (Zhang et al., 2006) and our preliminary result showed that ATP increased the frequency of miniature inhibitory postsynaptic potential (mIPSP) in acutely isolated neuron from substantia nigra, suggesting increased release of GABA from presynaptic terminal (unpublished data).

The enhancement of ATP-induced currents seemed to be associated with the ubiquitin ligase activity of parkin since it was not reproduced by a ligase-deficient mutant (Figs. 2C and 3). Involvement of the ubiquitin-proteasome system would accord with our previous observations with the ubiquitin hydrolase UCH-L1, though in this case hydrolase activity itself was not required since the effect of UCH-L1 was replicated by a hydrolase-deficient construct. Instead, upregulation of mono-ubiquitin (Osaka et al., 2003) and ubiquitin ligase activity of UCH-L1 (Liu et al., 2002) might be responsible for the potentiation of ATP-induced currents.

Though the precise mechanism how ubiquitin ligase activity of parkin is involved is not known yet, possible signaling leading to enhancement of the ATP-induced currents is summarized in Fig. 10. It is only a part of the mechanism revealed in the present investigation, because inhibition of PKA, CDK5 or phosphatases resulted in only partial ( $\pm 20\%$ ) inhibition of the parkin-potentiated currents which showed threefold increase in amplitude compared to control.

At least, part of the increase in ATP-induced currents appeared to result from activation of PKA directly or indirectly, because PKA inhibitor partially attenuated parkin-induced potentiation of ATP-currents (Fig. 7A). In a reverse way, activation of PKA by forskolin augmented the ATP-induced currents in mock-transfected cells (Manago et al., 2005). One possible mechanism would be phosphorylation of P2X receptors by PKA. It was reported that activation of PKA potentiated ATP-evoked current in P2X<sub>4</sub>-transfected HEK293 cells (Brown et al., 2004), while there was an opposite result in P2X<sub>2</sub>-transfected HEK293 cells (Chow and Wang, 1998). CaMKII could be activated by PKA indirectly via an inhibition of PP-1 (Winder and Sweatt, 2001), but KN-93 did not have any effect on ATP-induced currents in parkin-transfected cells (Fig. 7C), suggesting that CaMKII was not significantly activated by parkin.

Since the enhancement was not completely reversed by inhibition of PKA, other mechanisms must be involved. One such mechanism might be through modification of DARPP-32. In rat striatum, it has been suggested that there is positive and negative feedback regulation of DARPP-32 via activation of PKA and CDK5, respectively (Nishi et al., 2000). Since DARPP-32 was expressed in PC12 cells (Manago et al., 2005), its possible involvement was tested using roscovitine, a CDK5 inhibitor, and okadaic acid, a protein phosphatase (PP-1 and PP-2A) inhibitor. Roscovitine further enhanced the ATP-induced currents in parkin-transfected cells (Fig. 8A), suggesting a negative-feedback role for CDK5. It seemed likely that parkin stimulated CDK5 since roscovitine did not have significant effect on mock-transfected cells (Fig. 8C). On the other hand, a role for phosphatases was suggested by the fact that okadaic acid further enhanced the ATP-induced

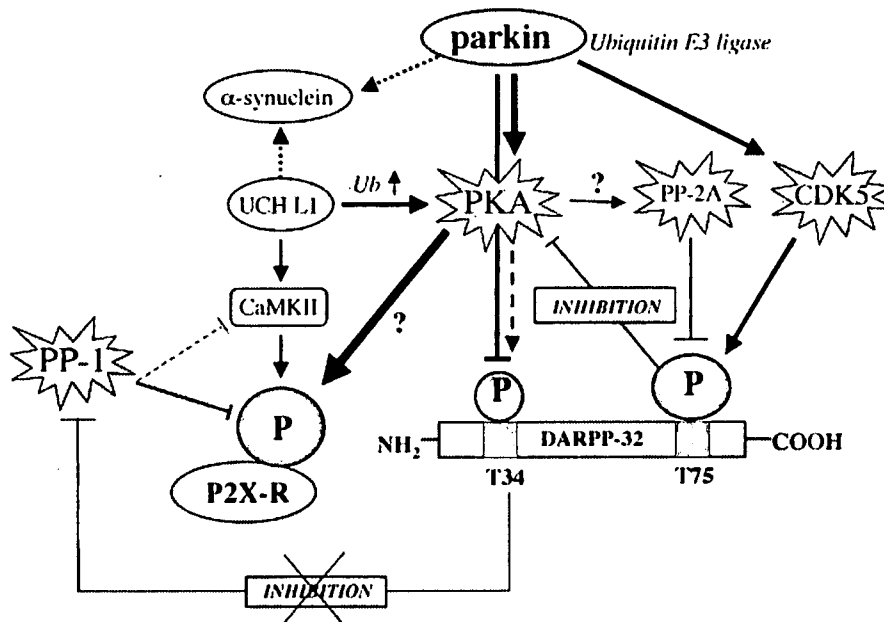


Fig. 10. Predicted signaling induced by expression of parkin. Parkin may activate PKA, subsequently phosphorylating P2X receptors. Parkin also may activate DARPP-32 at Thr-34. On the other hand, phosphorylation and dephosphorylation of DARPP-32 at Thr-75 by CDK5 and PP-2A could compete with each other, keeping the level of phospho Thr-75 unchanged. As additional information, ubiquitin C-terminal hydrolase (UCH-L1) also activates PKA, which is independent on hydrolase activity but presumably due to the increase

in mono-ubiquitin level (Manago et al., 2005) or ubiquitin ligase activity (Liu et al., 2002). Unlike parkin, UCH-L1 activates Ca<sup>2+</sup> and calmodulin-dependent protein kinase (CaMKII), which could be indirectly activated by PKA and dephosphorylated by PP-1 (Winder and Sweatt, 2001). The effect of  $\alpha$ -synuclein, a substrate for both parkin and UCH-L1 (dotted line), was not clear, because transfection of  $\alpha$ -synuclein did not affect ATP-induced currents. Reported signaling but not confirmed in the present study was shown by dotted line.

currents in parkin-transfected cells (Fig. 8B). Since inhibition of PP-2A was supposed to inhibit PKA activity (Nishi et al., 2000; Manago et al., 2005), it seemed likely that this enhancement resulted mainly from inhibition of PP-1. In mock-transfected cells, okadaic acid did not have significant effect (Fig. 8D).

As for the phosphorylation of DARPP-32, activation of PKA would phosphorylate DARPP-32 at Thr-34 (Nishi et al., 2000). However, the staining of phospho Thr-34 was rather attenuated in parkin-transfected cells (Fig. 9A), suggesting that parkin may have inhibitory effect on the phosphorylation site at Thr-34. Therefore, parkin might indirectly activate PP-1, canceling the negative feedback from phospho Thr-34. Concerning the phosphorylation of DARPP-32 at Thr-75, CDK5, and PP-2A were supposed to have opposite effects, keeping the same level of phospho Thr-75 (Fig. 9B).

Both UCH-L1 and parkin can operate via  $\alpha$ -synuclein as a target substrate (Shimura et al., 2001; Snyder and Wolozin, 2004). It has recently been shown that UCH-L1, parkin, and  $\alpha$ -synuclein form lysine 63-linked multiubiquitin chains, which induce proteasomal-independent ubiquitination (Doss-Pepe et al., 2005; Lim et al., 2005). Therefore, it was possible that  $\alpha$ -synuclein also had potentiating effect on P2X receptors if lysine 63-linked multiubiquitin was involved. However,  $\alpha$ -synuclein did not have such effect (Fig. 6). It will be great interest to investigate the relationship between these three proteins and it may help to understand why parkin deficient-mice are not a robust model of parkinsonism (Perez and Palmiter, 2005), though there were alterations in energy metabolism, protein handling, and synaptic function (Periquet et al., 2005).

Another interesting point is that the signaling between activation of PKA and potentiation of P2X receptors induced by either UCH-L1 or parkin was not the same. For example, UCH-L1 but not parkin activated CaMKII and PP-2A whereas parkin but not UCH-L1 seemed to activate CDK5, producing a negative feedback effect on PKA (Fig. 10). In addition, we found that DARPP-32 (phospho Thr-34) was rather attenuated in spite of the report that activation of PKA increased the phosphorylation at Thr-34 (Nishi et al., 2000). The difference between UCH-L1 and parkin might due to the different substrate specificity as ubiquitin ligases.

Unfortunately, the low transfection efficiency precluded direct biochemical studies on the phosphorylation or dephosphorylation of specific proteins by parkin or UCH-L1. As a result, we have been restricted to pharmacological and immunocytochemical analyses. Nevertheless, the important point we have established is that enzymes working in the ubiquitin-proteasome system have clear and substantial effects on a neurotransmitter receptor and hence subsequently may affect neurotransmission in vivo. It is widely accepted that there are number of diseases related to aberrations in the ubiquitin system (Ciechanover and Schwartz, 2004), but how aberrations in the ubiquitin system cause neurodegenerative diseases such as Parkinson's disease (PD) is largely unknown. In the present study, one of the ubiquitin ligases, parkin, potentiated the function of P2X receptors, as well as another enzyme working in the ubiquitin-proteasome system, UCH-L1. Presynaptic P2X receptors triggers  $Ca^{2+}$ -dependent glutamate release in the brainstem (Shigetomi and Kato, 2004), though ATP-mediated inhibition of dopamine release was reported in rat neostriatum (Trendelenburg and Bultmann, 2000). It is of great interest how endogenous

parkin or UCH-L1 modulates neurotransmitter release by stimulating P2X receptors in vivo, which is now under investigation.

## ACKNOWLEDGMENTS

We thank Ms. Yuki Kosai for technical assistance to get confocal images and Prof. David A. Brown (University College London, UK) for reading the manuscript and giving many useful comments. Grants-in Aid for Scientific Research of Japan Society for Promotion of Science (No. 15082214), Grants-in Aid for Scientific Research in Priority Area Research of the Ministry of Education, Culture, Sports, Science and Technology, Japan (No. 16300126), Grants-in-Aid for Scientific Research of the Ministry of Health, Labour and Welfare, Japan (H15-Kokoro-023, H17-Genome-009) and a grant from the Program for Promotion of Fundamental Studies in Health Sciences of the National Institute of Biomedical Innovation (NIBIO), Japan (05-32).

## LITERATURE CITED

- Brown DA, Bruce JI, Straub SV, Yule DI. 2004. cAMP potentiates ATP-evoked calcium signaling in human parotid acinar cells. *J Biol Chem* 279:39485-39494.
- Chow YW, Wang HL. 1998. Functional modulation of P2X2 receptors by cyclic AMP-dependent protein kinase. *J Neurochem* 70:2606-2612.
- Ciechanover A, Schwartz AL. 2004. The ubiquitin system: Pathogenesis of human diseases and drug targeting. *Biochim Biophys Acta* 1695:3-17.
- Cookson MR. 2005. The biochemistry of Parkinson's disease. *Annu Rev Biochem* 74:29-52.
- Doss-Pepe EW, Chen L, Madura K. 2005. Alpha-synuclein and parkin contribute to the assembly of ubiquitin lysine63-linked multiubiquitin chains. *J Biol Chem* 280:16619-16624.
- Hegde AN, Inokuchi K, Pei W, Casadio A, Ghirardi M, Chain DG, Martin KC, Kandel ER, Schwartz JH. 1997. Ubiquitin C-terminal hydrolase is an immediate-early gene essential for long-term facilitation in *Aplysia*. *Cell* 89:115-126.
- Hur EM, Park TJ, Kim KT. 2001. Coupling of L-type voltage-sensitive calcium channels to P2X(2) purinoceptors in PC-12 cells. *Am J Physiol Cell Physiol* 280:C1121-C1129.
- Huynh DP, Scoles DR, Nguyen D, Pulst SM. 2003. The autosomal recessive juvenile Parkinson disease gene product, parkin, interacts with and ubiquitinates synaptotagmin XI. *Hum Mol Genet* 12:2587-2597.
- Imai Y, Soda M, Takahashi R. 2000. Parkin suppresses unfolded protein stress-induced cell death through its E3 ubiquitin-protein ligase activity. *J Biol Chem* 275:35661-35664.
- Impey S, Obrietan K, Wong ST, Poser S, Yano S, Wayman G, Deloume JC, Chan G, Storm DR. 1998. Cross talk between ERK and PKA is required for  $Ca^{2+}$  stimulation of CREB-dependent transcription and ERK nuclear translocation. *Neuron* 21:869-883.
- Kitada T, Asakawa S, Hattori N, Matsumine H, Yamamura Y, Minoshima S, Yokochi M, Mizuno Y, Shimizu N. 1998. Mutations in the parkin gene cause autosomal recessive juvenile parkinsonism. *Nature* 392:605-608.
- Ko HS, von Coelln R, Sriram SR, Kim SW, Chung KK, Pletnikova O, Troncoso J, Johnson B, Saffary R, Goh EL, Song H, Park BJ, Kim MJ, Kim S, Dawson VL, Dawson TM. 2005. Accumulation of the authentic parkin substrate aminoacyl-tRNA synthetase cofactor, p38/JTV-1, leads to catecholaminergic cell death. *J Neurosci* 25:7968-7978.
- Kubo S, Kitami T, Noda S, Shimura H, Uchiyama Y, Asakawa S, Minoshima S, Shimizu N, Mizuno Y, Hattori N. 2001. Parkin is associated with cellular vesicles. *J Neurochem* 78:42-54.
- Lim KL, Chew KC, Tan JM, Wang C, Chung KK, Zhang Y, Tanaka Y, Smith W, Engelender S, Ross CA, Dawson VL, Dawson TM. 2005. Parkin mediates nonclassical, proteasomal-independent ubiquitination of Synphilin-1: Implications for Lewy body formation. *J Neurosci* 25:2002-2009.
- Liu Y, Fallon L, Lashuel HA, Liu Z, Lansbury PT Jr. 2002. The UCH-L1 gene encodes two opposing enzymatic activities that affect alpha-synuclein degradation and Parkinson's disease susceptibility. *Cell* 111:209-218.
- Manago Y, Kanahori Y, Shimada A, Sato A, Amano T, Sato-Sano Y, Setsuie R, Sakurai M, Aoki S, Wang YL, Osaka H, Wada K, Noda M. 2005. Potentiation of ATP-induced currents due to the activation of P2X receptors by ubiquitin carboxy-terminal hydrolase L1. *J Neurochem* 92:1061-1072.
- Min BI, Kim CJ, Rhee JS, Akaike N. 1996. Modulation of glycine-induced chloride current in acutely dissociated rat periaqueductal gray neurons by l-opioid agonist DAGO. *Brain Res* 734:72-78.
- Nakazawa K, Inoue K. 1992. Roles of  $Ca^{2+}$  influx through ATP-activated channels in catecholamine release from pheochromocytoma PC12 cells. *J Neurophysiol* 68:2026-2032.
- Nakazawa K, Inoue K, Koizumi S, Inoue K. 1994. Facilitation by 5-hydroxytryptamine of ATP-activated current in rat pheochromocytoma cells. *Pflügers Arch* 427:492-499.
- Nishi A, Bibb JA, Snyder GL, Higashi H, Nairn AC, Greengard P. 2000. Amplification of dopaminergic signaling by a positive feedback loop. *Proc Natl Acad Sci USA* 97:12840-12845.
- Noda M, Nakanishi H, Nabekura J, Akaike N. 2000. AMPA-kainate subtypes of glutamate receptor in rat cerebral microglia. *J Neurosci* 20:251-258.
- Osaka H, Wang YL, Takada K, Takizawa S, Setsuie R, Li H, Sato Y, Nishikawa K, Sun YJ, Sakurai M, Harada T, Hara Y, Kimura I, Chiba S, Namikawa K, Kiyama H, Noda M, Aoki S, Wada K. 2003. Ubiquitin carboxy-terminal

- hydrolase L1 binds to and stabilizes monoubiquitin in neuron. *Hum Mol Genet* 12:1945–1958.
- Perez FA, Palmiter RD. 2005. Parkin-deficient mice are not a robust model of parkinsonism. *Proc Natl Acad Sci USA* 102:2174–2179.
- Periquet M, Corti O, Jacquier S, Brice A. 2005. Proteomic analysis of parkin knockout mice: Alterations in energy metabolism, protein handling and synaptic function. *J Neurochem* 95:1259–1276.
- Sela D, Ram E, Atlas D. 1991. ATP receptor. A putative receptor-operated channel in PC-12 cells. *J Biol Chem* 266:17990–17994.
- Shimura H, Hattori N, Kubo S, Mizuno Y, Asakawa S, Minooshima S, Shimizu N, Iwai K, Chiba T, Tanaka K, Suzuki T. 2000. Familial Parkinson disease gene product, parkin, is a ubiquitin-protein ligase. *Nat Genet* 25:302–305.
- Shimura H, Schlossmacher MG, Hattori N, Froesch MP, Trockenbacher A, Schneider R, Mizuno Y, Kosik KS, Selkoe DJ. 2001. Ubiquitination of a new form of alpha-synuclein by parkin from human brain: Implications for Parkinson's disease. *Science* 293:263–269.
- Snyder H, Wolozin B. 2004. Pathological proteins in Parkinson's disease: Focus on the proteasome. *J Mol Neurosci* 24:425–442.
- Shigetomi E, Kato F. 2004. Action potential-independent release of glutamate by  $Ca^{2+}$  entry through presynaptic P2X receptors elicits postsynaptic firing in the brainstem autonomic network. *J Neurosci* 24:3125–3135.
- Sriram SR, Li X, Ko HS, Chung KK, Wong E, Lim KL, Dawson VL, Dawson TM. 2005. Familial-associated mutations differentially disrupt the solubility, localization, binding and ubiquitination properties of parkin. *Hum Mol Genet* 14:2571–2586.
- Trendelenburg AU, Bultmann R. 2000. P2 receptor-mediated inhibition of dopamine release in rat neostriatum. *Neuroscience* 96:249–252.
- Winder DG, Sweatt JD. 2001. Roles of serine/threonine phosphatases in hippocampal synaptic plasticity. *Nat Rev Neurosci* 2:461–474.
- Zhang Y, Gao J, Chung KK, Huang H, Dawson VL, Dawson TM. 2000. Parkin functions as an E2-dependent ubiquitin-protein ligase and promotes the degradation of the synaptic vesicle-associated protein, CDCrel-1. *Proc Natl Acad Sci USA* 97:13354–13359.
- Zhang Y, Deng P, Li Y, Xu ZC. 2006. Enhancement of excitatory synaptic transmission in spiny neurons after transient forebrain ischemia. *J Neurophysiol* 95:1537–1544.



# Degradation of Amyotrophic Lateral Sclerosis-linked Mutant Cu,Zn-Superoxide Dismutase Proteins by Macroautophagy and the Proteasome<sup>\*[S]</sup>

Received for publication, April 7, 2006, and in revised form, August 18, 2006. Published, JBC Papers in Press, August 18, 2006, DOI 10.1074/jbc.M603337200

Tomohiro Kabuta, Yasuyuki Suzuki, and Keiji Wada<sup>1</sup>

From the Department of Degenerative Neurological Diseases, National Institute of Neuroscience, National Center of Neurology and Psychiatry, Kodaira, Tokyo 187-8502, Japan

Mutations in the Cu,Zn-superoxide dismutase (SOD1) gene cause ~20% of familial cases of amyotrophic lateral sclerosis (fALS). Accumulating evidence indicates that a gain of toxic function of mutant SOD1 proteins is the cause of the disease. It has also been shown that the ubiquitin-proteasome pathway plays a role in the clearance and toxicity of mutant SOD1. In this study, we investigated the degradation pathways of wild-type and mutant SOD1 in neuronal and nonneuronal cells. We provide here the first evidence that wild-type and mutant SOD1 are degraded by macroautophagy as well as by the proteasome. Based on experiments with inhibitors of these degradation pathways, the contribution of macroautophagy to mutant SOD1 clearance is comparable with that of the proteasome pathway. Using assays that measure cell viability and cell death, we observed that under conditions where expression of mutant SOD1 alone does not induce toxicity, macroautophagy inhibition induced mutant SOD1-mediated cell death, indicating that macroautophagy reduces the toxicity of mutant SOD1 proteins. We therefore propose that both macroautophagy and the proteasome are important for the reduction of mutant SOD1-mediated neurotoxicity in fALS. Inhibition of macroautophagy also increased SOD1 levels in detergent-soluble and -insoluble fractions, suggesting that both detergent-soluble and -insoluble SOD1 are degraded by macroautophagy. These findings may provide further insights into the mechanisms of pathogenesis of fALS.

Amyotrophic lateral sclerosis (ALS)<sup>2</sup> is a neurodegenerative disease caused by selective loss of motor neurons (1, 2).

\* This work was supported by grants-in-aid for scientific research from the Japan Society for the Promotion of Science; a research grant in a priority area of research from the Ministry of Education, Culture, Sports, Science, and Technology, Japan; grants-in-aid for scientific research from the Ministry of Health, Labor and Welfare, Japan; and the Program for Promotion of Fundamental Studies in Health Sciences of the National Institute of Biomedical Innovation, Japan. The costs of publication of this article were defrayed in part by the payment of page charges. This article must therefore be hereby marked "advertisement" in accordance with 18 U.S.C. Section 1734 solely to indicate this fact.

[S] The on-line version of this article (available at <http://www.jbc.org>) contains supplemental Figs. S1–S6.

<sup>1</sup> To whom correspondence should be addressed: Dept. of Degenerative Neurological Diseases, National Institute of Neuroscience, National Center of Neurology and Psychiatry, 4-1-1 Ogawahigashi, Kodaira, Tokyo 187-8502, Japan. Tel: 81-42-346-1715; Fax: 81-42-346-1745; E-mail: wada@ncnp.go.jp.

<sup>2</sup> The abbreviations used are: ALS, amyotrophic lateral sclerosis; fALS, familial ALS; SOD1, Cu,Zn-superoxide dismutase(s); 3-MA, 3-methyladenine; siRNA, short interfering RNA; EGFP, enhanced green fluorescent protein; HA, hemag-

glutinin; MTS, 3-(4,5-dimethylthiazol-2-yl)-5-(3-carboxymethoxyphenyl)-2-(4-sulfophenyl)-2H-tetrazolium.

Although most cases of ALS are sporadic, ~10% of ALS cases run in families. Dominant missense mutations in the gene that encodes the Cu,Zn-superoxide dismutase (SOD1) are responsible for 20% of familial ALS (fALS) cases (3). Mice overexpressing mutant SOD1 develop an ALS-like phenotype comparable with human ALS, whereas mice lacking SOD1 do not (4, 5). These findings have led to the conclusion that SOD1 mutants cause motor neuron degeneration by a toxic gain of function. Thus, studies of the degradation process of mutant SOD1 proteins could provide important insights into understanding the mechanisms that underlie the pathology of fALS, and possibly sporadic ALS, and into developing novel therapies for fALS by removing toxic species of mutant SOD1.

Cytoplasmic proteins are mainly degraded by two pathways, the ubiquitin-26 S proteasome pathway (6) and autophagy (7). Previous studies have shown that mutant SOD1 proteins are turned over more rapidly than wild-type SOD1, and a proteasome inhibitor increases the level of mutant SOD1 proteins (8, 9). Dorfin and NEDL1, two distinct ubiquitin ligases, ubiquitinate mutant but not wild-type SOD1 (10, 11). These observations suggest that mutant SOD1 is degraded by the ubiquitin-26 S proteasome pathway and that the increased turnover of mutant SOD1 is mediated in part by this pathway. On the other hand, the 20 S proteasome, a component of the 26 S proteasome, can degrade proteins without a requirement for ubiquitination (12, 13). A recent study has found that metal-free forms of wild-type and mutant SOD1 are degraded by the 20 S proteasome *in vitro* (14).

Autophagy is an intracellular process that results in the degradation of cytoplasmic components inside lysosomes. At least three forms of autophagy have been described in mammalian cells: macroautophagy, microautophagy, and chaperone-mediated autophagy (7). Macroautophagy is the major and the most well studied form of autophagy; this process begins with a sequestration step, in which cytosolic components are engulfed by a membrane sac called the isolation membrane. This membrane results in a double membrane structure called the autophagosome, which fuses with the lysosome. The inner membrane of the autophagosome and its protein and organelle contents are degraded by lysosomal hydrolases. Recent reports have demonstrated that macroautophagy plays an important role in preventing neurodegeneration in mice (15, 16). Although macroautophagy can be induced by starvation, this

pathway may take place constitutively in mammals (17). In cultured cells, inhibition of macroautophagy does not alter enhanced green fluorescent protein (EGFP) levels (18) or glyceraldehyde-3-phosphate dehydrogenase protein levels,<sup>3</sup> suggesting that not all cytosolic proteins are degraded by macroautophagy. To date, however, there have been no reports of macroautophagy in mutant SOD1 clearance.

In this study, we investigated the pathway by which human wild-type SOD1 and the A4V, G85R, and G93A SOD1 mutants are degraded in neuronal and nonneuronal cells. We show that wild-type and mutant SOD1 proteins are degraded by both the proteasomal pathway and macroautophagy. The experiments with inhibitors of these degradation pathways suggested that mutant SOD1 are degraded more rapidly than wild-type SOD1 in part by macroautophagy and that the contribution of macroautophagy to mutant SOD1 clearance is approximately equal to that of the proteasome pathway. Macroautophagy decreases mutant SOD1 protein levels in both nonionic detergent-soluble and -insoluble fractions. In addition, we provide data indicating that macroautophagy has a role in mutant SOD1-mediated cell death.

## EXPERIMENTAL PROCEDURES

**Plasmid Constructs**—The expression plasmids pcDNA3-hSOD1 containing wild-type, A4V, G85R, and G93A mutant SOD1 were kindly donated by Ryosuke Takahashi (Kyoto University, Kyoto, Japan) and Makoto Urushitani (Laval University, Quebec, Canada) (19). To construct a plasmid expressing human wild-type SOD1 with the HA tag at the carboxyl terminus of SOD1, HA-tagged SOD1 fragments were amplified by PCR using wild-type SOD1 cDNA (Open Biosystems, Huntsville, AL) as the template. The PCR products were digested with XhoI and NotI and cloned into an XhoI-NotI-digested pCI-neo vector (Promega, Madison, WI). The primers used were 5'-AAACTCGAGCCGCAAGATGGCGACGAAGGCCGTGTGCG-3' and 5'-AAAAGCGGCCGCTTAAGCGTATCTGGAACATCGTATGGGTATTGGGCGATCCCAATTACACCACA-3'. A plasmid expressing HA-tagged G93A SOD1 was generated using QuikChange site-directed mutagenesis kit (Stratagene, La Jolla, CA) according to the manufacturer's protocol. To construct a plasmid expressing fusion protein of green fluorescent protein and LC3, LC3 fragments were amplified by PCR using rat LC3 cDNA (Open Biosystems) as the template. The PCR products were digested with BglII and EcoRI and cloned into a BglII-EcoRI-digested pEGFP-C1 vector (Clontech). The primers used were 5'-ACTCAGATCTATGCCGTCGAGAAGACCTCAAAA-3' and 5'-TGCAGAATTCTTACACAGCCAGTGCTGTCCCGAA-3'. After construction, the DNA sequences of the plasmids were confirmed by DNA sequence analysis.

**Cell Culture and Transfection**—The mouse neuroblastoma cell line Neuro2a, the human neuroblastoma cell line SH-SY5Y, and the monkey kidney-derived cell line COS-7 were maintained in Dulbecco's modified Eagle's medium (Sigma) supplemented with 10% fetal calf serum (JRH Biosciences, Lenexa, KS). Transient expression of each vector in Neuro2a and COS-7 cells was performed using the FuGENE 6 transfection reagent

(Roche Applied Science). For experiments with differentiated Neuro2a cells, the medium was changed to differentiation medium (Dulbecco's modified Eagle's medium supplemented with 1% fetal calf serum and 20  $\mu$ M retinoic acid) 24 h after transfection. Approximately 90% of cells in dishes (wells) were transfected in our experimental conditions (data not shown), and there was no notable differences in the transfection efficiency among the wells (supplemental Fig. S1).

**Treatment of Cells with Epoxomicin, 3-Methyladenine, Cycloheximide, Rapamycin, or NH<sub>4</sub>Cl**—Cells grown in 12- or 6-well plates to 50–80% confluence were transfected with expression plasmids containing wild-type, A4V, G85R, or G93A mutant SOD1. 24 h after transfection, cells were incubated with epoxomicin (10 nM, 1  $\mu$ M, 5  $\mu$ M, or 10  $\mu$ M; Sigma), 3-methyladenine (3-MA) (10, 20, or 30 mM; Sigma), rapamycin (100 or 200 nM; Sigma), 20 mM NH<sub>4</sub>Cl, and/or carrier (Me<sub>2</sub>SO or water) as a control. In some experiments, 10  $\mu$ g/ml cycloheximide (Sigma) was added to the cells to avoid the confounding effects of ongoing protein synthesis. Epoxomicin, cycloheximide, and rapamycin were dissolved in Me<sub>2</sub>SO, NH<sub>4</sub>Cl in water. 3-MA was freshly dissolved in culture medium 30 min before use.

**Cell Fractionation**—For preparation of nonionic detergent-soluble and -insoluble fractions, adherent cells were harvested and lysed on ice for 15 min in 1% Triton X-100 lysis buffer containing 50 mM Tris-HCl, pH 7.5, 150 mM NaCl, 5 mM EDTA, 1% Triton X-100, and protease inhibitors (Complete, EDTA-free; Roche Applied Science). Lysates were centrifuged at 20,000  $\times$  g for 10 min at 4  $^{\circ}$ C, and the supernatants were pooled and designated as the detergent-soluble fractions. After the pellets were washed with 1% Triton X-100 lysis buffer, they were solubilized with SDS buffer (50 mM Tris-HCl, pH 7.5, 150 mM NaCl, 5 mM EDTA, 3% SDS, 1% Triton X-100, and protease inhibitors) and sonicated. The resulting solution was used as the detergent-insoluble fraction. For preparation of total cell lysates containing both detergent-soluble and -insoluble fractions, cells were lysed in SDS buffer and sonicated. Protein concentrations were determined with the protein assay kit (Bio-Rad) or the DC protein assay kit (Bio-Rad).

**Western Blot Analysis**—Western blotting was performed using standard procedures as described previously (20). The primary antibodies used were as follows: anti-SOD1 rabbit polyclonal antibody (1:4000; Stressgen Bioreagents, Victoria, Canada), anti- $\alpha$ -tubulin mouse monoclonal antibody (1:4000; Sigma), anti- $\beta$ -actin mouse monoclonal antibody (1:5000; Sigma), anti-HA mouse monoclonal antibody (1:4000; Sigma), anti-Beclin 1 mouse monoclonal antibody (1:500; BD Transduction Laboratories, San Diego, CA), anti-Apg7/Atg7 rabbit polyclonal antibody (1:500; Rockland, Gilbertsville, PA). After overnight incubation with primary antibodies at 4  $^{\circ}$ C, each blot was probed with horseradish peroxidase-conjugated anti-rabbit IgG or anti-mouse IgG (1:20,000; Pierce). Immunoreactive signals were visualized with SuperSignal West Dura extended duration substrate (Pierce) or SuperSignal West Femto maximum sensitivity substrate (Pierce) and detected with a chemiluminescence imaging system (FluorChem; Alpha Innotech, San Leandro, CA). The signal intensity was quantified by densitometry using FluorChem software (Alpha Innotech).

**Short Interfering RNA (siRNA) Preparation and Transfection**—Double-stranded siRNA targeting mouse Beclin 1, mouse Atg7 and EGFP were purchased from RNAi Co., Ltd.

<sup>3</sup> T. Kabuta, Y. Suzuki, and K. Wada, unpublished data.

## Degradation of Mutant SOD1 by Macroautophagy

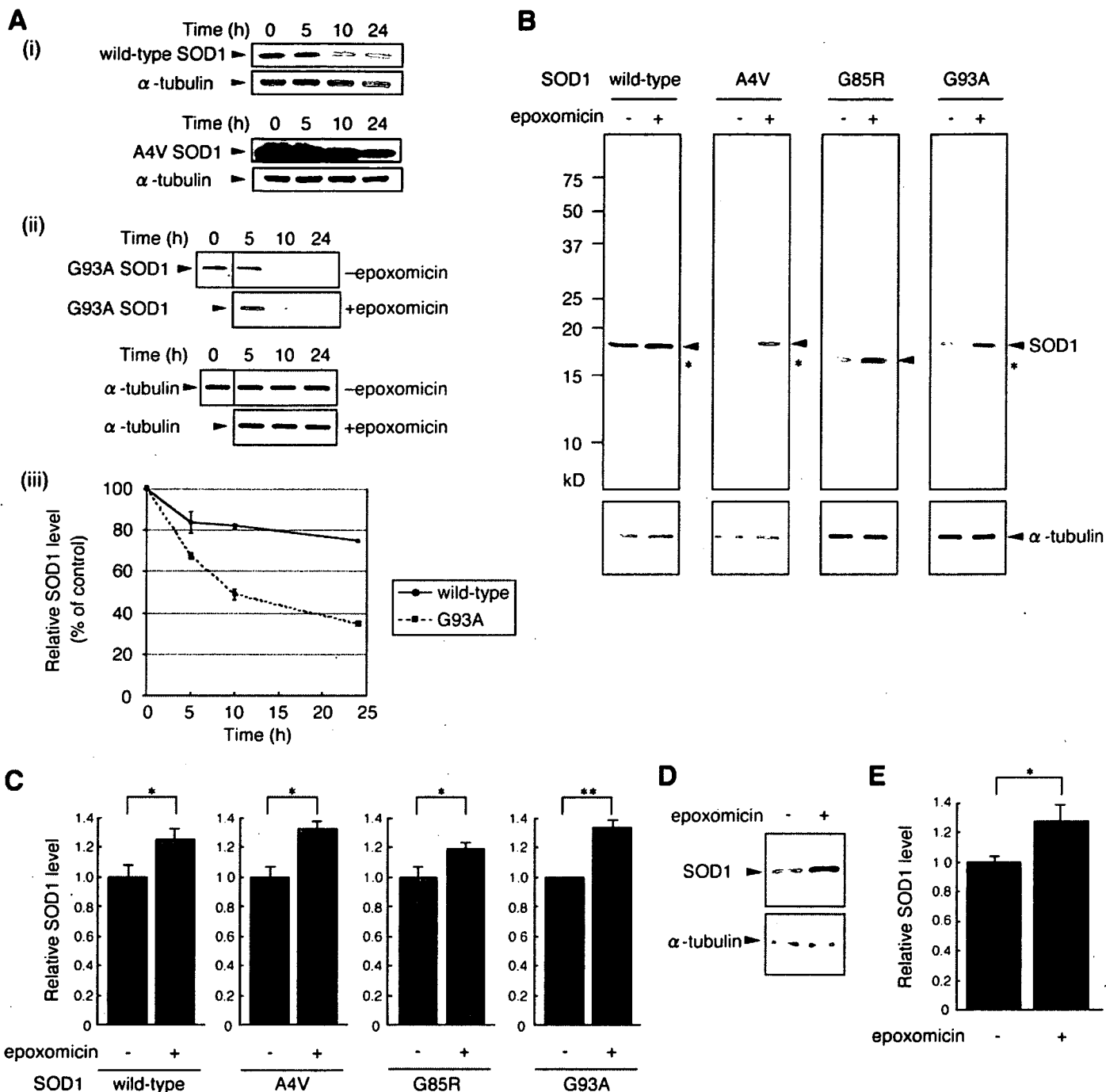


**FIGURE 1. Both mutant and wild-type SOD1 are degraded by the proteasome.** *A, i*, Neuro2a cells were transiently transfected with wild-type or mutant A4V human SOD1. 24 h after transfection, cells were treated with 10  $\mu$ g/ml cycloheximide for the indicated time and lysed. Total cell lysates were analyzed by immunoblotting using anti-SOD1 or anti- $\alpha$ -tubulin antibody. *ii*, Neuro2a cells transfected with G93A SOD1 were incubated with or without 10 nM epoxomicin in the presence of 10  $\mu$ g/ml cycloheximide for the indicated time and lysed. Total cell lysates were analyzed by immunoblotting using anti-SOD1 or anti- $\alpha$ -tubulin antibody. *iii*, the relative levels of wild-type or G93A SOD1 (percentage of 0-h control) were quantified by densitometry. Mean values are shown with S.E. ( $n = 3$ ). *B* and *C*, Neuro2a cells were transiently transfected with wild-type or mutant A4V, G85R, or G93A human SOD1. 24 h after transfection, cells were incubated with or without 10 nM epoxomicin in the presence of 10  $\mu$ g/ml cycloheximide for 24 h. Total cell lysates were analyzed by immunoblotting using anti-SOD1 antibody. The electrophoretic mobility of G85R SOD1 was greater than that of wild-type SOD1.  $\alpha$ -Tubulin was used as a loading control. Asterisks indicate endogenous mouse SOD1 (*B*). The relative level of wild-type or mutant SOD1 was quantified by densitometry. Mean values are shown with S.E. ( $n = 3$ ). \*,  $p < 0.05$ ; \*\*,  $p < 0.01$  (*C*). *D* and *E*, human SH-SY5Y cells were incubated with or without 10 nM epoxomicin in the presence of cycloheximide for 24 h. Total cell lysates were analyzed by immunoblotting with anti-SOD1 antibody (*D*). The relative level of human endogenous SOD1 was quantified by densitometry. Data are expressed as the means  $\pm$  S.E. ( $n = 3$ ). \*,  $p < 0.05$  (*E*).

(Tokyo, Japan). Sequences targeted by siRNA were selected using siDirect (RNAi Co., Ltd.): mouse Beclin 1 siRNA, sense (5'-GUC-UACAGAAAGUGCUAAUAG-3') and antisense (5'-AUUAGC-ACUUUCUGUAGACAU-3'); mouse Atg7 siRNA, sense (5'-GAGCGGCGGCUGGUAAGAACA-3') and antisense (5'-UUC-

UUACCAGCCGCCGCUCUA-3'); EGFP siRNA, sense (5'-GCC-ACAACGUCUAUAUCAUGG-3') and antisense (5'-AUGAUA-UAGACGUUGUGGCUG-3'). EGFP siRNA was used as a control. Cells ( $3 \times 10^5$ ) were cotransfected with 1  $\mu$ g of DNA and 3  $\mu$ g of siRNA using Lipofectamine PLUS reagent (Invitrogen).

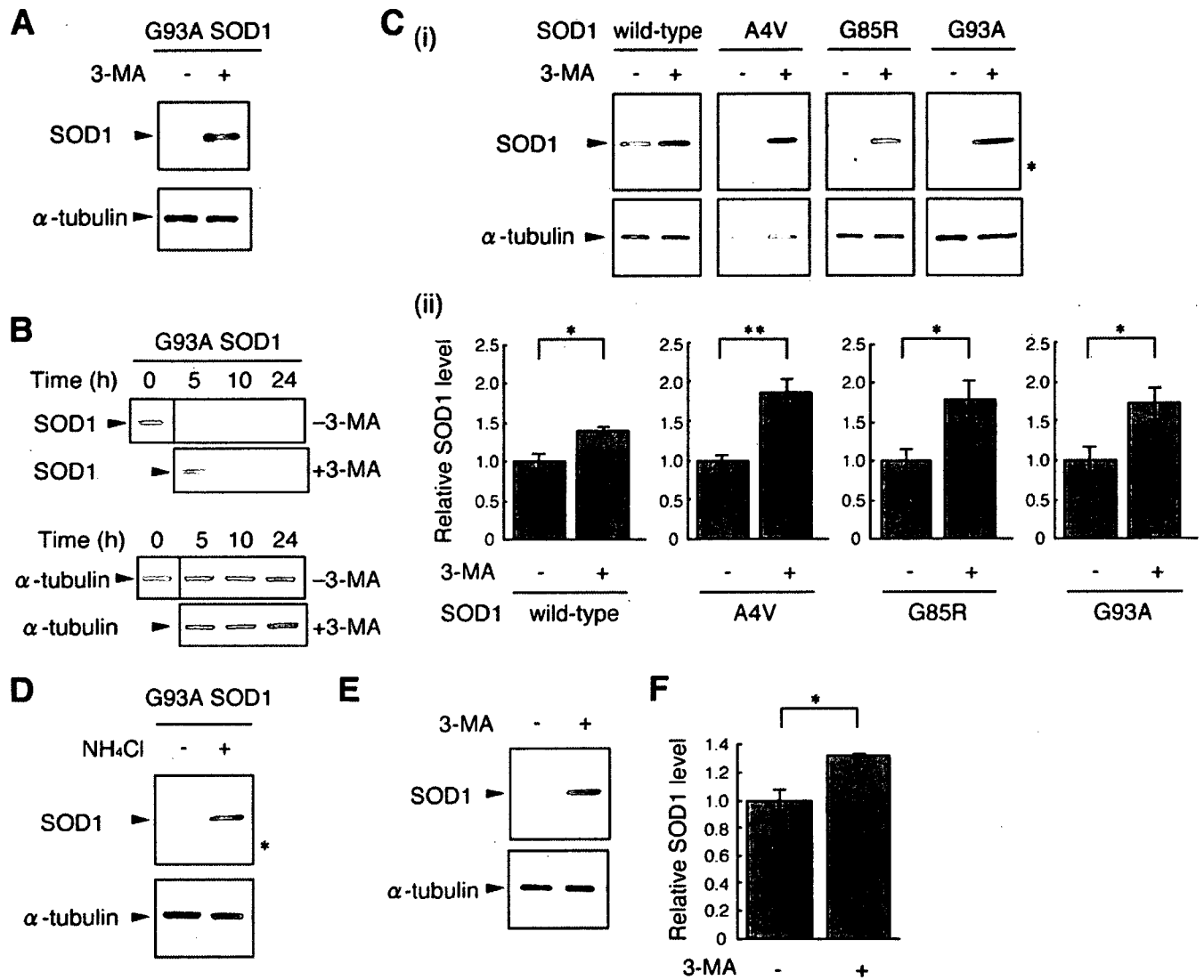


**FIGURE 2. Wild-type and mutant SOD1 are degraded by macroautophagy.** *A*, Neuro2a cells were transiently transfected with the G93A mutant SOD1. 24 h after transfection, cells were incubated with or without 10 mM 3-MA for 24 h. Total cell lysates were analyzed by immunoblotting using anti-SOD1 antibody.  $\alpha$ -Tubulin was used as a loading control. *B*, Neuro2a cells transfected with G93A SOD1 were incubated with or without 10 mM 3-MA in the presence of 10  $\mu$ g/ml cycloheximide for the indicated time and lysed. Total cell lysates were analyzed by immunoblotting using anti-SOD1 or anti- $\alpha$ -tubulin antibody. *C*, Neuro2a cells transfected with wild-type or mutant A4V, G85R, or G93A SOD1 were incubated with or without 10 mM 3-MA in the presence of 10  $\mu$ g/ml cycloheximide for 24 h. Total cell lysates were analyzed by immunoblotting. An asterisk indicates endogenous mouse SOD1 (*i*). The relative level of wild-type or mutant SOD1 was quantified by densitometry. Mean values are shown with S.E. ( $n = 3$ ). \*,  $p < 0.05$ ; \*\*,  $p < 0.01$  (*ii*). *D*, Neuro2a cells transfected with G93A SOD1 were incubated with or without 20 mM  $\text{NH}_4\text{Cl}$  in the presence of cycloheximide for 24 h. Total cell lysates were analyzed by immunoblotting. An asterisk indicates endogenous mouse SOD1. *E* and *F*, 5H-SY5Y cells were incubated with or without 10 mM 3-MA in the presence of cycloheximide for 24 h. Total cell lysates were analyzed by immunoblotting (*E*). The relative level of human endogenous SOD1 was quantified by densitometry. Data are expressed as the means  $\pm$  S.E. ( $n = 3$ ). \*,  $p < 0.05$  (*F*).

**Quantitative Assessment of Cell Viability and Cell Death**—One day before transfection, Neuro2a cells were seeded at  $5 \times 10^4$  cells/well in 24-well plates. 24 h after transfection with 0.4  $\mu$ g of DNA/well, cells were cultured in differentiation medium with or without 10 mM 3-MA for 24 h. Cell death was assessed by a lactate dehydrogenase release assay using the CytoTox-ONE homogeneous membrane integrity assay (Promega) according to the manufacturer's protocol. The percentage of cytotoxicity (Fig. 7G) was calculated according to this protocol. For assessment of cell viability, we used the 3-(4,5-dimethylthiazol-2-yl)-5-(3-carboxymethoxyphenyl)-2-(4-sulfophenyl)-2H-tetrazolium (MTS) assay and the ATP assay with the CellTiter 96 AQueous One Solution cell proliferation assay (Promega) and CellTiter-Glo luminescent cell viability assay (Promega), respectively, according to

the manufacturer's protocols. Measurements with a multiplate reader were performed after samples were transferred to 96-well assay plates.

**Statistical Analysis**—For comparison of two groups, the statistical difference was determined by Student's *t* test. For comparison of more than two groups, analysis of variance was used. If the analysis of variance was significant, Dunnett's multiple comparison test was used as a *post hoc* test.

**RESULTS**

**Wild-type and Mutant SOD1 Are Degraded by the Proteasome**—To determine whether SOD1 is degraded by the proteasome pathway, we assessed the effect of proteasome inhibitors on SOD1 protein clearance. Peptide aldehydes, such as